






Dysfunction of exhausted T cells is enforced by MCT11-mediated lactate metabolism

Received: 12 December 2023

Accepted: 2 October 2024

Published online: 8 November 2024

 Check for updates

Ronal M. Peralta^{1,2}, Bingxian Xie^{1,2}, Konstantinos Lontos^{2,3}, Hector Nieves-Rosado^{1,2}, Kellie Spahr^{1,2}, Supriya Joshi^{1,2}, B. Rhodes Ford^{1,4}, Kevin Quann³, Andrew T. Frisch^{1,2}, Victoria Dean^{1,2}, Mary Philbin², Anthony R. Cillo ^{1,2,5}, Sebastian Gingras ¹, Amanda C. Poholek ^{1,4}, Lawrence P. Kane ^{1,2}, Dayana B. Rivadeneira ^{1,2} & Greg M. Delgoffe ^{1,2} ✉

CD8⁺ T cells are critical mediators of antitumor immunity but differentiate into a dysfunctional state, known as T cell exhaustion, after persistent T cell receptor stimulation in the tumor microenvironment (TME). Exhausted T (T_{ex}) cells are characterized by upregulation of coinhibitory molecules and reduced polyfunctionality. T cells in the TME experience an immunosuppressive metabolic environment via reduced levels of nutrients and oxygen and a buildup of lactic acid. Here we show that terminally T_{ex} cells uniquely upregulate *Slc16a11*, which encodes monocarboxylate transporter 11 (MCT11). Conditional deletion of MCT11 in T cells reduced lactic acid uptake by T_{ex} cells and improved their effector function. Targeting MCT11 with an antibody reduced lactate uptake specifically in T_{ex} cells, which, when used therapeutically in tumor-bearing mice, resulted in reduced tumor growth. These data support a model in which T_{ex} cells upregulate MCT11, rendering them sensitive to lactic acid present at high levels in the TME.

CD8⁺ T cells have a crucial role in orchestrating immune responses against pathogens and tumors. Antigen recognition via the T cell receptor (TCR) promotes activation and expansion of a clonal army to target infected or malignant cells¹. Upon antigen clearance, most effector cells die, leaving a population of memory T cells which will become reactivated upon encountering their cognate antigen². However, when antigen persists and T cells are exposed to continuous TCR stimulus, as in the context of cancer, they progressively differentiate into a hypofunctional state known as T cell exhaustion³. At least two distinct populations have been identified in the exhaustion lineage: progenitor exhausted (T_{pex}) cells and terminally differentiated exhausted (T_{ex}) cells⁴. T_{pex} cells are characterized by intermediate expression of PD1 and retention of self-renewal capacities maintained via the transcription factor TCF-1 (ref. 5). As TCR stimulation persists, T_{pex} cells ultimately become T_{ex} cells, which are characterized by a reduction in self-renewal capacity and ability to produce effector cytokines (that is, IL-2 and TNF) and upregulation of coinhibitory molecules (that is,

PD1, CTLA-4, Tim3 and Lag3)³. Persistent stimulation by antigen leads CD8⁺ T cells infiltrating the tumor to differentiate to T_{ex} cells, ultimately contributing to tumor immune escape.

While persistent TCR stimulus may be the main driver of T cell exhaustion, metabolic stress, especially in the context of the tumor microenvironment (TME), can also promote dysfunction in T_{ex} cells⁶. Rapidly dividing cancer cells outgrow their vasculature, leading to poorly oxygenated regions within the tumor⁷, which can promote T cell exhaustion^{8,9}. Cancer cells are highly metabolically active and outcompete T cells for essential metabolites¹⁰, while also secreting metabolic byproducts into the extracellular space. One of the most abundant metabolites in the TME is lactic acid, which cancer and stromal cells export as an end product of aerobic glycolysis¹¹. This leads to a reduction in extracellular pH, which inhibits T cell function^{12,13}. As T cell function and differentiation are intrinsically linked to various metabolic pathways, many approaches target pathways to modulate the metabolic milieu of the TME and promote antitumor immunity¹⁴.

¹Department of Immunology, University of Pittsburgh, Pittsburgh, PA, USA. ²Tumor Microenvironment Center, UPMC Hillman Cancer Center, Pittsburgh, PA, USA. ³Department of Medicine, Division of Hematology/Oncology, University of Pittsburgh, Pittsburgh, PA, USA. ⁴Department of Pediatrics, University of Pittsburgh, Pittsburgh, PA, USA. ⁵Center for Systems Immunology, University of Pittsburgh, Pittsburgh, PA, USA. ✉e-mail: gdelgoffe@pitt.edu

It remains important to understand metabolic drivers of dysfunction in tumor-infiltrating CD8⁺ T_{ex} cells to propel development of cancer treatments.

While the abundance of a metabolite in the extracellular environment is important, cells require transporters to exchange most metabolites through the plasma membrane. Metabolite transporters act as gatekeepers of metabolism, giving cells access to exchange metabolites with their environment. Members of the solute carrier (SLC) superfamily play critical roles in transporting a host of different metabolites, either into—or out of—an organelle or cell¹⁵. SLCs are critical in shaping the metabolic landscape of the TME, as cancer cells use these transporters to secrete metabolic end products that can suppress antitumor immunity¹⁶. Expression of SLCs in cancer cells enables them to outcompete immune cells for essential metabolites¹⁷. Which SLCs are expressed in subsets of tumor-infiltrating CD8⁺ T cells, how these SLCs affect their metabolism and whether their expression can influence differentiation into exhaustion remains unstudied.

Here, we show that tumor-infiltrating T_{ex} cells highly upregulate the *Slc16* monocarboxylate transporter (MCT) *Slc16a11* (MCT11), enabling increased uptake of monocarboxylates (such as lactic acid) upon tumor infiltration. While expression of MCT11 could be upregulated by chronic TCR stimulus, exposure to hypoxia drove greater and sustained MCT11 expression, dependent on Hif1 α . Deletion of MCT11 in endogenous T cells resulted in improved effector functions within T_{ex} cells and synergy with α PD1 therapy. Given the effects of conditional knockout of MCT11 in T cells, we treated tumor-bearing mice with MCT11-blocking monoclonal antibodies and found that the blockade of MCT11 could lead to clearances as a monotherapy but could also synergize with α PD1. Thus, this study suggests SLCs can be targeted on immune cells for therapeutic benefit.

Results

T_{ex} cells express MCT11, promoting lactic acid metabolism

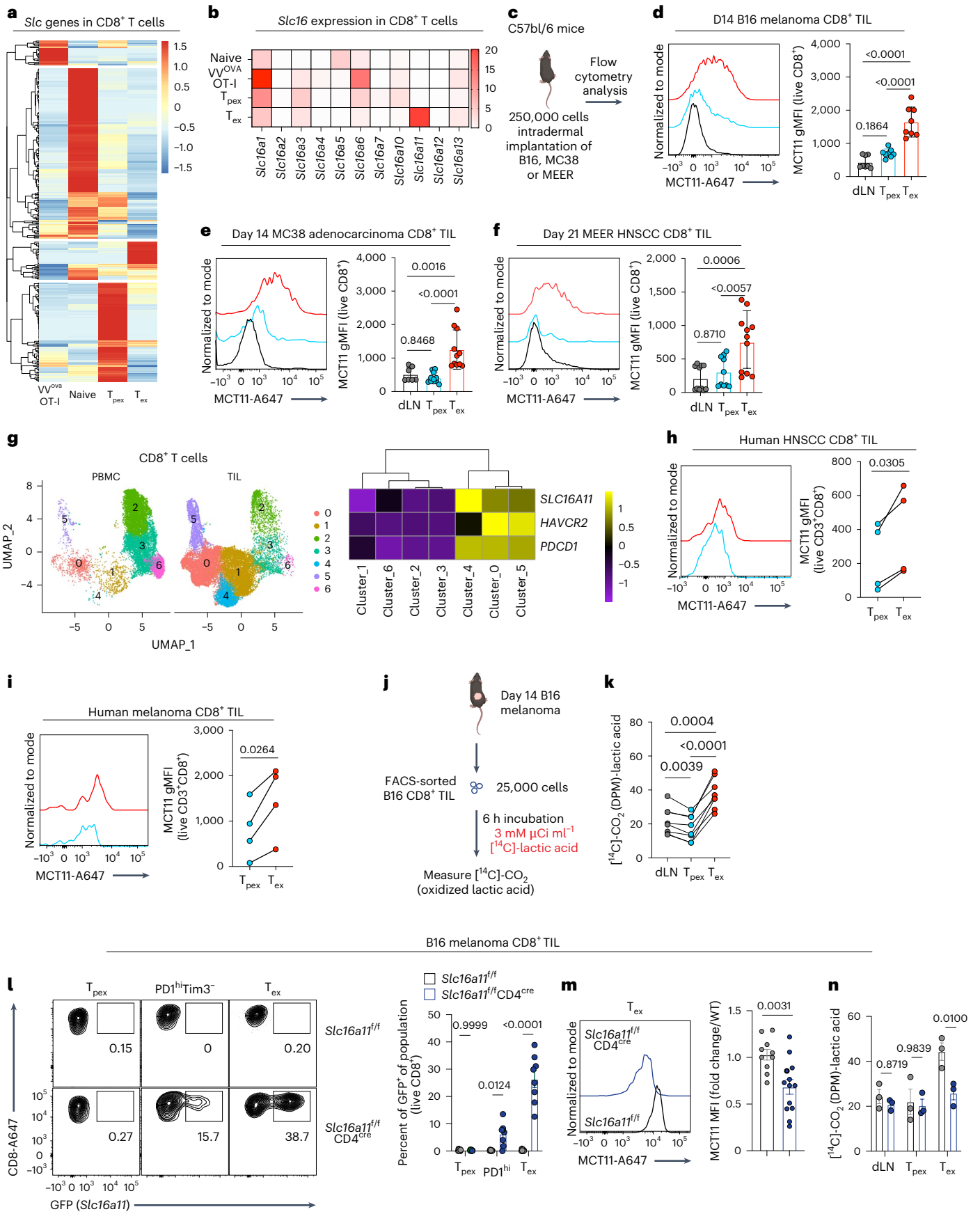
T_{ex} cells exist in a state of metabolic dysfunction in the TME, due to disrupted mitochondrial biogenesis¹⁸, hypoxia¹⁹ and competition with tumor cells for essential metabolites^{10,17}. As cells take up a substantial proportion of their metabolites using members of the SLC superfamily²⁰, we sought to determine which SLCs were expressed in tumor-infiltrating T_{ex} cells. We compared the transcriptome of splenic OT-1 (transgenic T cell with TCR specific to ovalbumin (OVA)) effector T cells responding to vaccinia^{OVA}, tumor-draining lymph node (dLNs) naive CD8⁺ T cells, T_{pe} cells (CD8⁺PD1^{int}Tim3⁺Slamf6^{hi}TOX^{int}) and T_{ex} cells (CD8⁺PD1^{hi}Tim3⁺Slamf6^{lo}TOX^{hi}) from murine B16 melanoma tumors (Extended Data Figs. 1 and 2a–d)²¹. SLCs were differentially expressed during distinct stages of activation, highlighting that various subsets are engaged in distinct metabolic processes requiring a unique set of transporters (Fig. 1a). Consistent with the notion that T cells compete poorly for nutrients in the TME, T_{ex} cells repressed the

majority of SLCs (Fig. 1a). However, a subset of SLCs were preferentially expressed in T_{ex} cells. One of the most differentially expressed SLCs in T_{ex} cells is a member of the *Slc16* MCT family, *Slc16a11* (MCT11), the dominant MCT expressed in T_{ex} cells (Fig. 1b). In fact, *Slc16a11* was one of the most differentially expressed genes when comparing T_{ex} with T_{pe} cells and was enriched more than canonical exhaustion genes such as *Tox*, *Ifng* and *Gzmb* (Extended Data Fig. 2b). Flow cytometric analysis using a mouse and/or human cross-reactive antibody on CD8⁺ tumor infiltrating lymphocytes (TIL) from B16, MC38 and MEER (a model of human papillomavirus-positive head and neck squamous cell carcinoma (HNSCC)) revealed MCT11 to be highly expressed on the surface of T_{ex} cells (Fig. 1c–f). Analysis of previously published^{22,23} single-cell sequencing data from human CD8⁺ intratumoral T cells showed that human T_{ex} cells also expressed *SLC16A11*, with a particularly high expression in HNSCC-infiltrating CD8⁺ T cells coexpressing *HAVCR2* and *PDCD1*, with minimal representation of these clusters in peripheral blood mononuclear cells (PBMCs) (Fig. 1g). We confirmed the expression of MCT11 protein on the surface of human T_{ex} cells from HNSCC and melanoma via flow cytometry (Fig. 1h,i). Using previously published single-cell sequencing data²⁴, we were able to identify *SLC16A11* upregulation in T_{ex} cells from various human cancers. *SLC16A11* expression was upregulated in T_{ex} cells from pancreatic cancer, multiple myeloma, ovarian cancer and renal cancer (Extended Data Fig. 2g)²⁴. These data highlight MCT11 as a novel surface protein on tumor-infiltrating T_{ex} cells.

MCT11 is a member of the *Slc16* family, which are MCTs that mediate transport of metabolites such as pyruvate, lactate and ketone bodies²⁵. MCT11 was first described in 2014; polymorphisms in the gene led to susceptibility to type 2 diabetes²⁶. Through various follow up studies^{27,28}, it has been shown that MCT11 is a proton-coupled type-1 MCT that is chaperoned to the cell surface by basigin, also known as CD147 (ref. 27), and highly expressed in T_{ex} cells (Extended Data Fig. 2e)²⁹. We have previously shown regulatory T cells in the TME take up and metabolize lactic acid via *Slc16a1* (MCT1)³⁰, so we investigated whether T_{ex} cells could take up lactic acid through MCT11, as lactic acid is present in high concentrations in the TME^{11,31}. We first overexpressed MCT11 in wild-type (WT) CD8⁺ T cells and pulsed these cells with [¹⁴C]-lactate to measure its uptake and oxidation to [¹⁴C]-CO₂ (Extended Data Fig. 3a,b). [¹⁴C]-lactate uptake and oxidation to CO₂ was increased in MCT11 overexpressing cells over empty vector (EV)-expressing controls (Extended Data Fig. 3c,d), indicating lactate was being taken and metabolized through the tricarboxylic acid (TCA) cycle in MCT11-expressing cells. Next, we asked whether there was a difference in ability to metabolize lactic acid in CD8⁺ TIL populations. We sorted T_{ex} and T_{pe} cells from B16 melanoma tumors, as well as dLN CD8⁺ T cells and pulsed them with [¹⁴C]-lactate for 6 h (Fig. 1j). We found T_{ex} cells, which express MCT11, had increased [¹⁴C]-lactate oxidation to [¹⁴C]-CO₂, compared with T_{pe} cells, which do not express it (Fig. 1k).

Fig. 1 | MCT11 expression enables lactic acid metabolism in T_{ex} cells. **a**, SLC superfamily gene expression from bulk RNA-seq in splenic OT-1 T cells responding to vaccinia^{OVA}, tumor dLN naive CD8⁺ T cells and B16-infiltrating T_{pe} (PD1^{int}Tim3⁺Slamf6^{hi}TOX^{int}) and T_{ex} (PD1^{hi}Tim3⁺Slamf6^{lo}TOX^{hi}) CD8⁺ T cells. **b**, *Slc16* family gene transcripts per million in CD8⁺ T cell groups. **c**, A total of 250,000 B16, MC38 or MEER cells were intradermally implanted on C57BL/6 mice. **d–f**, A representative histogram and geometric mean fluorescence intensity (gMFI) quantification of MCT11 surface expression from ex vivo CD8⁺ T cells collected from day 14. **d–f**, B16 melanoma ($n = 8$) (**d**), MC38 colorectal cancer ($n = 10$) (**e**) and day 21 MEER HNSCC-bearing mice ($n = 11$) (**f**). **g**, *Slc16a11* expression from single-cell sequencing in CD8⁺ T cell populations in human PBMC- and HNSCC-infiltrating CD8⁺ T cells^{22,23}. **h,i**, Representative histogram and quantification of MCT11 expression in CD8⁺ TIL from human HNSCC ($n = 4$) (**h**) and melanoma ($n = 4$) (**i**). **j**, Experimental outline of [¹⁴C]-lactic acid oxidation, where 25,000 B16 dLN CD8⁺ T cells and tumor-infiltrating T_{pe} and T_{ex} cells were sorted by fluorescence activated cell sorting (FACS) and cultured for 6 h in [¹⁴C]-lactic acid to measure the

amount converted to [¹⁴C]-CO₂. **k**, [¹⁴C]-lactic acid oxidation converted to [¹⁴C]-CO₂ in disintegrations per minute (dpm) in dLN CD8⁺ T cells and tumor-infiltrating T_{pe} and T_{ex} cells ($n = 7$). *Slc16a11*^{fl/fl}CD4^{cre} ($n = 8$) and *Slc16a11*^{fl/fl} littermate controls ($n = 8$) were implanted with B16 and sacrificed on day 14. **l**, Representative flow cytometry plots and quantification of MCT11 (via GFP expression) in T_{pe}, PD1^{hi} and T_{ex} T cell populations in *Slc16a11*^{fl/fl}CD4^{cre} ($n = 8$) and *Slc16a11*^{fl/fl} mice ($n = 8$). **m**, A representative histogram and mean fluorescence intensity (MFI) quantification of MCT11 in T_{ex} cells from *Slc16a11*^{fl/fl}CD4^{cre} ($n = 13$) and *Slc16a11*^{fl/fl} mice ($n = 10$). **n**, [¹⁴C]-lactic acid oxidation in dLN CD8⁺ T cells and B16-infiltrating T_{pe} and T_{ex} cells from *Slc16a11*^{fl/fl}CD4^{cre} ($n = 3$) and *Slc16a11*^{fl/fl} ($n = 3$) mice. The data represent three independent experiments for **d–f**, **l** and **n** and four for **h**, **i**, **k** and **m**. The error bars indicate the mean \pm the standard error of the mean. The statistical analysis was performed by a one-way ANOVA with Tukey's multiple comparisons test for **d–f** and **k**, paired two-tailed Student's *t*-tests for **h** and **i**, two-way ANOVA with Sidák's multiple comparison for **l** and **n** or unpaired two-tailed Student's *t*-tests for **m**. Panels **c** and **j** were created with BioRender.com.



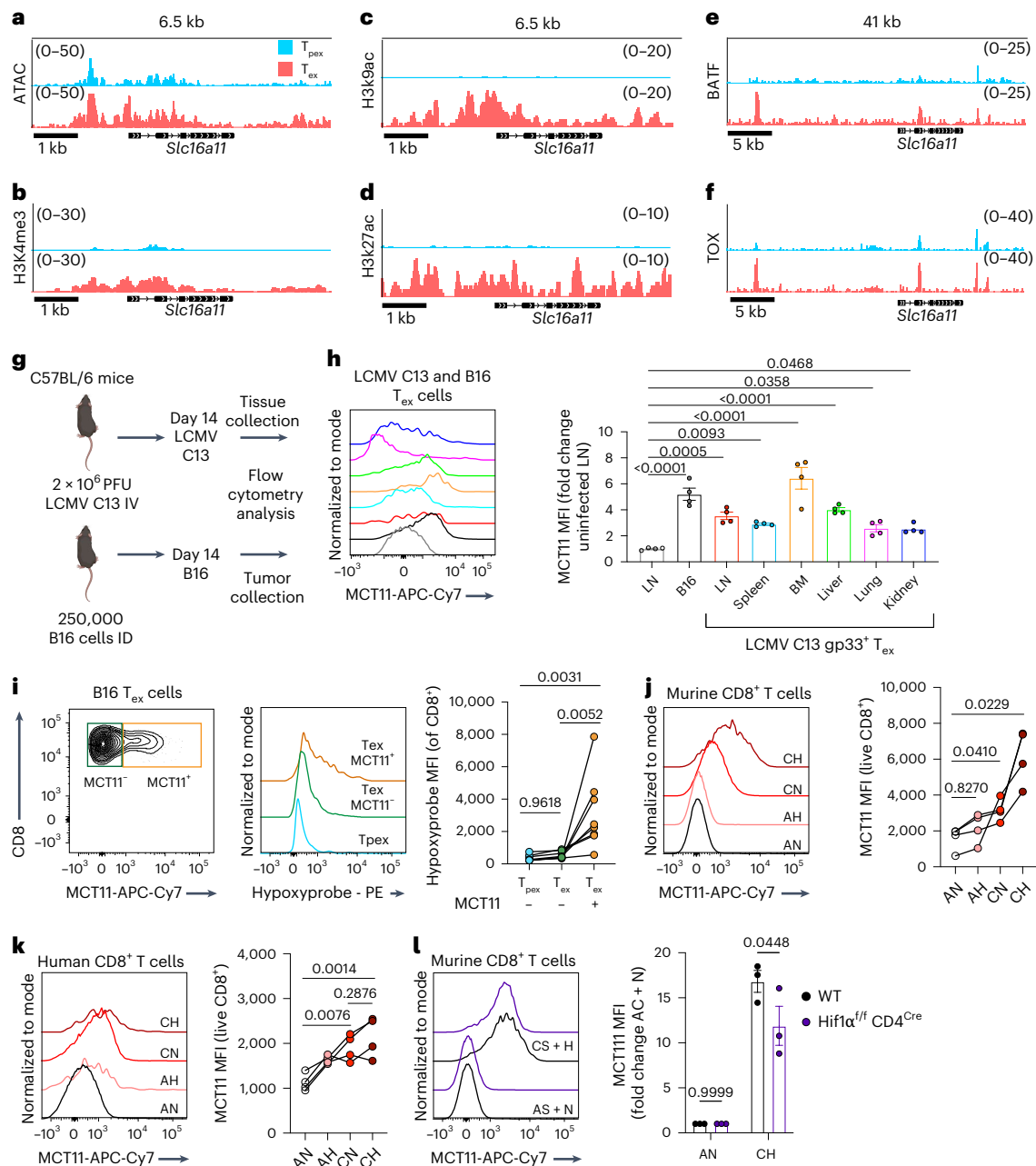


Fig. 2 | MCT11 expression is driven by continuous TCR stimulation. **a**, ATAC sequencing of the *Slc16a11* locus in T_{pex} and T_{ex} cells responding to B16-F10 (ref. 4). **b–f**, CUT&RUN of H3K4me3 (**b**), H3K9ac (**c**), H3K27ac (**d**), BATF (**e**) and Tox (**f**) at the *Slc16a11* locus in B16 melanoma-infiltrating T_{pex} and T_{ex} cells²¹. **g**, C57BL/6 mice were intravenously (IV) infected with 2 × 10⁶ PFU of LCMV C13 or intradermally (ID) implanted with 250,000 B16 melanoma cells. A total of 14 days later, LN, spleen, BM, liver, lung and kidney were collected from LCMV C13-infected mice, and the tumors were collected from B16 melanoma-bearing mice. **h**, A representative histogram and quantification of MCT11 surface expression from ex vivo T_{ex} cells isolated from B16 melanoma-bearing mice ($n = 4$) or tissues from LCMV C13-infected mice ($n = 4$). **i**, Hypoxia experienced by D14 B16 melanoma-infiltrating CD8⁺ T cells expressing surface MCT11 ($n = 7$). **j**, A representative histogram and quantification of MCT11 surface expression in

murine CD8⁺ T cells cultured under acute stim (A, 1:1 stimulatory beads to T cell ratio for 24 h) and normoxia (N, 20% O₂), A and hypoxia (H, 1.5% O₂), continuous stim (C, 10:1 stimulatory beads to T cell ratio for 6 days) and N, or C and H ($n = 4$). **k**, A representative histogram and quantification of MCT11 surface expression of human CD8⁺ T cells cultured under the previously described conditions ($n = 4$). **l**, A representative histogram and quantification of MCT11 expression on CD8⁺ from WT ($n = 3$) and *Hif1 α ^{ff} CD4^{Cre}* ($n = 3$) mice cultured in C + H. The data represent two independent experiments for **h** and three for **i–l**. The error bars indicate the mean ± the standard error of the mean. The statistical analysis was performed by a repeated measures one-way ANOVA with Dunnett's multiple comparison for **h**, one-way ANOVA with Tukey's multiple comparison for **i–k** or two-way ANOVA with Šidák's multiple comparison for **l**. MFI, mean fluorescence intensity. Panel **g** was created with [BioRender.com](https://www.biorender.com).

To further understand the role of MCT11 in T_{ex} cell biology, we generated a conditional knockout by inversion (COIN)³² *Slc16a11*^{if/ff} mouse. This system works by targeting a gene of interest and interrupting its transcription by inverting a COIN module into an exon of the gene. We did this by inserting an artificial intron with a T2A-eGFP COIN module

into the fourth exon of the *Slc16a11* antisense strand, flanked by lox71 and lox66 and splicing sequences. Without Cre activity, the COIN module is spliced out, generating WT *Slc16a11* mRNA and protein. Under Cre activity, lox66 and lox71 flanking enables the inversion of the T2A-eGFP COIN module into the fourth exon of *Slc16a11* (ref. 33),

generating a truncated nonfunctional MCT11 protein and reporting of this event via green fluorescent protein (GFP) expression (Extended Data Fig. 4a). We, thus, generated a system where we could knockout the function of MCT11 and identify would-be MCT11-expressing cells by GFP fluorescence.

First, we generated a *Slc16a11*^{wt/f}CMV^{cre} line, which carry one functional allele of the gene, and searched for MCT11 expression via GFP fluorescence in tumor-infiltrating immune cells. Analysis of day 14 B16-infiltrating immune cells from *Slc16a11*^{wt/f}CMV^{cre} mice confirmed that CD8⁺ T cells expressed MCT11. Further, MCT11 was not expressed by other tumor-infiltrating immune cells, as tumor-infiltrating CD4⁺ T cells, B cells, natural killer cells, dendritic cells, polymorphonuclear-myleoid derived suppressor cells (PMN-MDSCs), monocytic-myleoid derived suppressor cells (M-MDSCs) and neutrophils (Extended Data Fig. 4). *Slc16a11*^{fl/fl} mice were crossed with *CD4*^{cre} mice to generate a T cell-conditional knockout. As expected, because *Slc16a11* is not expressed until T cells reach terminal exhaustion, there were no differences in development and function directly ex vivo (Extended Data Fig. 5a,b). Analysis of GFP expression in CD8⁺ TIL subsets from B16-bearing *Slc16a11*^{fl/fl} and *Slc16a11*^{fl/fl}CD4^{cre} mice confirmed our previous findings that MCT11 was expressed in T_{ex} cells (~25% of cells) but not T_{pe} cells (Fig. 1l). In addition, this analysis revealed that MCT11 expression begins in PD1^{hi}Tim3⁻ cells, during the transition from progenitor to terminal exhaustion (Fig. 1l). Antibody staining confirmed knockout of MCT11 in T_{ex} cells from *Slc16a11*^{fl/fl}CD4^{cre} (Fig. 1m). We then asked whether T_{ex} cells lacking MCT11 have a reduced ability to oxidize lactic acid. Indeed, conditional deletion of MCT11 led to decreased lactic acid oxidation in T_{ex} cells, reducing it essentially to the level of T_{pe} cells (Fig. 1n). Thus, T_{ex} cells uniquely upregulate MCT11, which enables the flux and metabolism of monocarboxylates, such as lactic acid.

MCT11 expression is driven by chronic TCR stimulus

Given the distinct expression of MCT11 in T_{ex} cells in tumors, we next wanted to determine what drove *Slc16a11* expression by examining the epigenetic landscape of its locus. An analysis of previously published⁴ ATAC sequencing revealed *Slc16a11* was more accessible in T_{ex} than T_{pe} cells from B16 tumors (Fig. 2a). Further, analysis of our previously published²¹ CUT&RUN data showed that the locus of *Slc16a11* in T_{ex} cells harbors the permissive histone modifications H3K4me3, H3K9ac and H3K27ac but not in T_{pe} cells (Fig. 2b–d). In addition, the *Slc16a11* locus is active and bound by the exhaustion-associated transcription factors BATF and TOX in T_{ex} cells (Fig. 2e,f). We next asked whether MCT11 expression was exclusive to tumor-infiltrating T_{ex} cells. Lymphocytic choriomeningitis virus clone 13 (LCMV C13) is a chronic viral infection that has been widely used to study T cell exhaustion. Given that LCMV C13 is a systemic infection, we searched for MCT11 expression in T_{ex} cells from different tissues of LCMV C13-infected mice and compared it with B16-infiltrating T_{ex} cells (Fig. 2g). We found that MCT11 was expressed in T_{ex} cells from the lymph nodes (LNs), spleen, kidney, liver, lung and bone

marrow (BM) of LCMV C13-infected mice at varying levels of expression in the different tissues (Fig. 2h). These data highlight MCT11 expression as part of the T cell exhaustion program and suggested there may be tissue specific factors further driving the expression of MCT11 in T_{ex} cells. The highest expression of MCT11 was in LCMV C13 T_{ex} cells from the BM, a tissue with hypoxic niches, such as tumors^{34,35}. Our lab and others have shown that T_{ex} cells experience higher levels of hypoxia in the TME than T_{pe} cells (Extended Data Fig. 2f)^{8,19,36,37}. Therefore, we investigated the levels of hypoxia experienced by MCT11⁺ T_{ex} cells by injecting B16-bearing mice with pimonidazole, a hypoxia tracer³⁸. We found MCT11⁺ T_{ex} cells had greater hypoxia exposure than MCT11⁻ T_{ex} cells (Fig. 2i), suggesting hypoxia could be a tissue specific factor that promotes MCT11 expression. To explore this in a reductionist fashion, we cultured CD8⁺ T cells under continuous TCR stimulus (protocol previously published), sufficient to drive an exhausted-like state (Extended Data Fig. 6), which drove MCT11 expression in murine and human CD8⁺ T cells (Fig. 2j,k). MCT11 expression was increased further when T cells receiving continuous TCR stimulus were cultured under hypoxia (Fig. 2j,k). Given the increased expression of MCT11 under hypoxia, we hypothesized that Hif1 α may promote expression of MCT11 in T_{ex} cells. While CD8⁺ T cells from *Hif1 α* ^{fl/fl}CD4^{cre} upregulated MCT11 when cultured under chronic TCR stimulus and hypoxia, there was a significant decrease in MCT11 expression when compared with WT CD8⁺ T cells (Fig. 2l), consistent with previous findings that *Hif1 α* is not solely responsible for hypoxia-induced potentiation of T cell exhaustion. Altogether, our data suggest that the core exhaustion program primes the *Slc16a11* locus for expression, and exposure to tissue factors such as hypoxia, through *Hif1 α* , further promotes MCT11 expression.

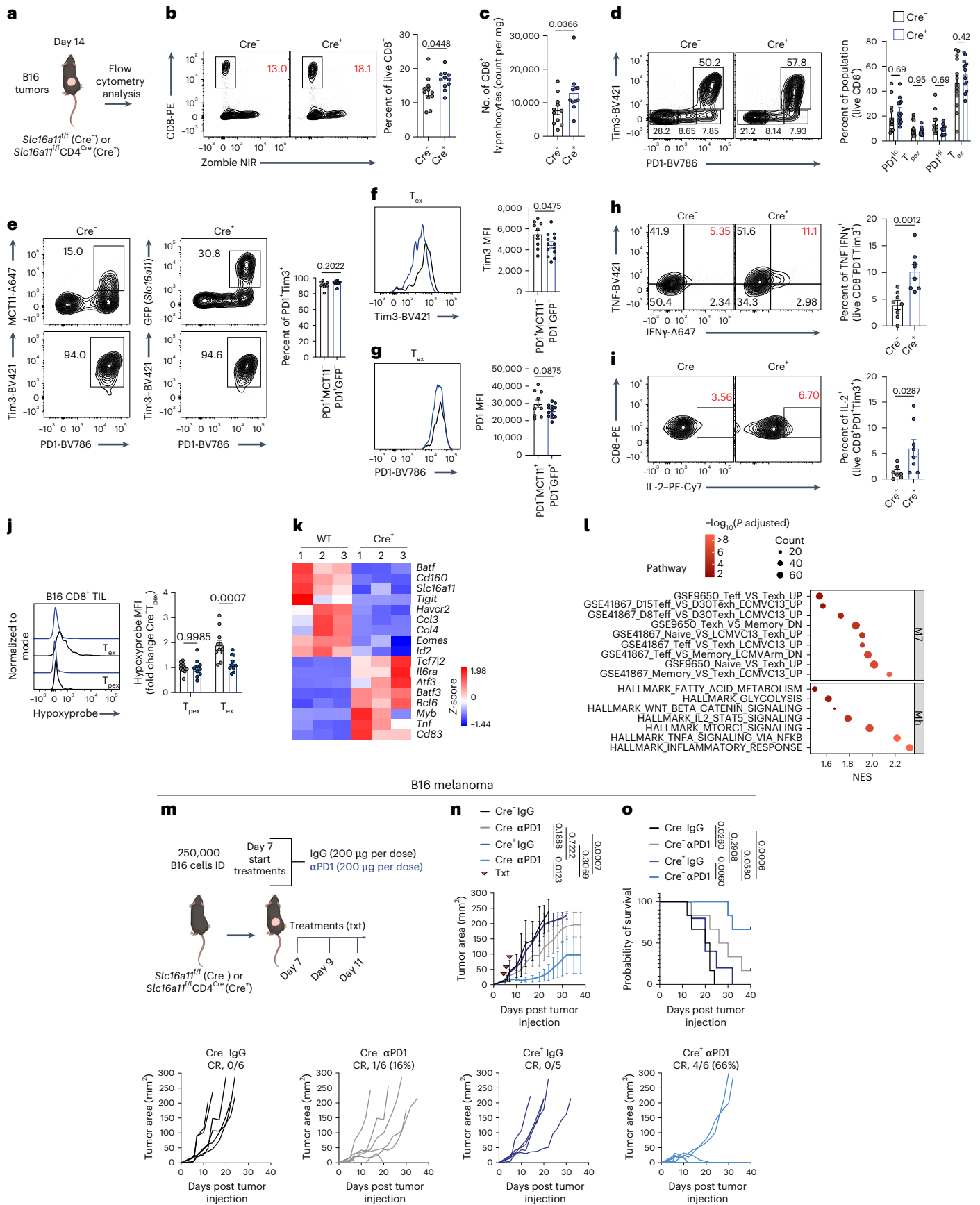
MCT11 enforces dysfunction in T_{ex} cells

We next sought to determine the contribution of MCT11-mediated metabolite uptake in the function and fate of T_{ex} cells. First, we retrovirally overexpressed MCT11 in OT-I (Thy1.1) T cells before adoptive transfer into B16^{OVA}-bearing mice (Thy1.2) (Extended Data Fig. 7a). Overexpression of MCT11 resulted in accelerated functional exhaustion, as these T cells had decreased TNF and interferon γ (IFN γ) production, although no appreciable changes were observed in tumor infiltration or coinhibitory marker expression when compared with EV controls (Extended Data Fig. 7b–d). These data suggested that MCT11, and by extension lactate uptake, could be driving dysfunction within T_{ex} cells.

To further interrogate the role of MCT11 in T cell exhaustion, we inoculated *Slc16a11*^{fl/fl} and *Slc16a11*^{fl/fl}CD4^{cre} mice with B16 melanoma and studied the infiltrating TIL via flow cytometry (Fig. 3a). Tumors from *Slc16a11*^{fl/fl}CD4^{cre} mice had a significant increase in infiltrating CD8⁺ T cells by percentage and total counts (Fig. 3b,c). MCT11 deficiency in CD8⁺ T cells did not lead to any numerical changes in the PD1^{lo}, T_{pe}, PD1^{hi} and T_{ex} populations (Fig. 3d), suggesting T cells still progressed to an exhausted surface phenotype. However, as not all T_{ex} cells express MCT11, we compared the exhaustion profile of GFP⁺ T_{ex} cell population from *Slc16a11*^{fl/fl}CD4^{cre} mice to MCT11⁺ T_{ex} cells from *Slc16a11*^{fl/fl} controls.

Fig. 3 | MCT11 enforces dysfunction in T_{ex} cells. **a**, *Slc16a11*^{fl/fl}CD4^{cre} (Cre⁺) and littermate *Slc16a11*^{fl/fl} (Cre⁻) controls were injected with 250,000 B16 melanoma and sacrificed on day 14 for tumor collection and flow cytometry analysis. **b,c**, Representative flow cytometry plots and quantification of percentage (**b**) and total counts of live CD8⁺ T cells infiltrating B16 tumors (**c**) in Cre⁻ ($n = 11$) and Cre⁺ mice ($n = 11$). **d**, A representative flow cytometry plot and quantification of PD1 and Tim3 populations in ex vivo B16 melanoma-infiltrating CD8⁺ T cells in Cre⁻ ($n = 12$) and Cre⁺ mice ($n = 13$). **e**, A representative flow cytometry plot and quantification of T_{ex} cells in PD1⁺MCT11⁺ and PD1⁺GFP⁺ T cells from Cre⁻ ($n = 10$) and Cre⁺ ($n = 13$) mice, respectively. **f,g**, Representative histograms and quantification of Tim3 (**f**) and PD1 MFI (**g**) in PD1⁺MCT11⁺ and PD1⁺GFP⁺ T cells from Cre⁻ ($n = 10$) and Cre⁺ ($n = 13$) mice, respectively. **h,i**, A representative flow cytometry plot and quantification of TNF and IFN γ (**h**) and IL-2 (**i**) in B16-infiltrating T_{ex} cells from Cre⁻ ($n = 8$) and Cre⁺ mice ($n = 8$) after 6 h of stimulation

with α CD3 (3 μ g ml⁻¹) and α CD28 (2 μ g ml⁻¹). **j**, A representative cytogram and quantification of hypoxypromin in T_{pe} and T_{ex} cells from Cre⁻ and Cre⁺ mice. **k**, Heat map of differentially expressed genes between T_{ex} cells from B16 tumors on Cre⁺ and WT mice. **l**, A gene set enrichment analysis of selected immunologic signature and hallmark gene sets in Cre⁺ T_{ex} cells over WT T_{ex} cells. A multiple comparisons correction was performed using the Benjamini–Hochberg method. **m**, Cre⁺ and Cre⁻ mice were intradermally (ID) implanted with 100,000 tumor cells and treated (txt) on days 7, 9 and 11 with α PD1 or isotype control mAb. **n,o**, Tumor growth with complete responses (CR) (**n**) and survival curve (**o**) of B16 melanoma on Cre⁻ and Cre⁺ mice. The data represent three independent experiments. The error bars indicate the mean \pm the standard error of the mean. The statistical analysis was performed by unpaired two-tailed Student's t -tests for **b**, **c** and **e–i**, by a two-way ANOVA with Tukey's multiple comparison for **d**, **j** and **n** or by a log rank Mendel–Cox test for **o**. Panels **a** and **m** were created with [BioRender.com](https://www.biorender.com).



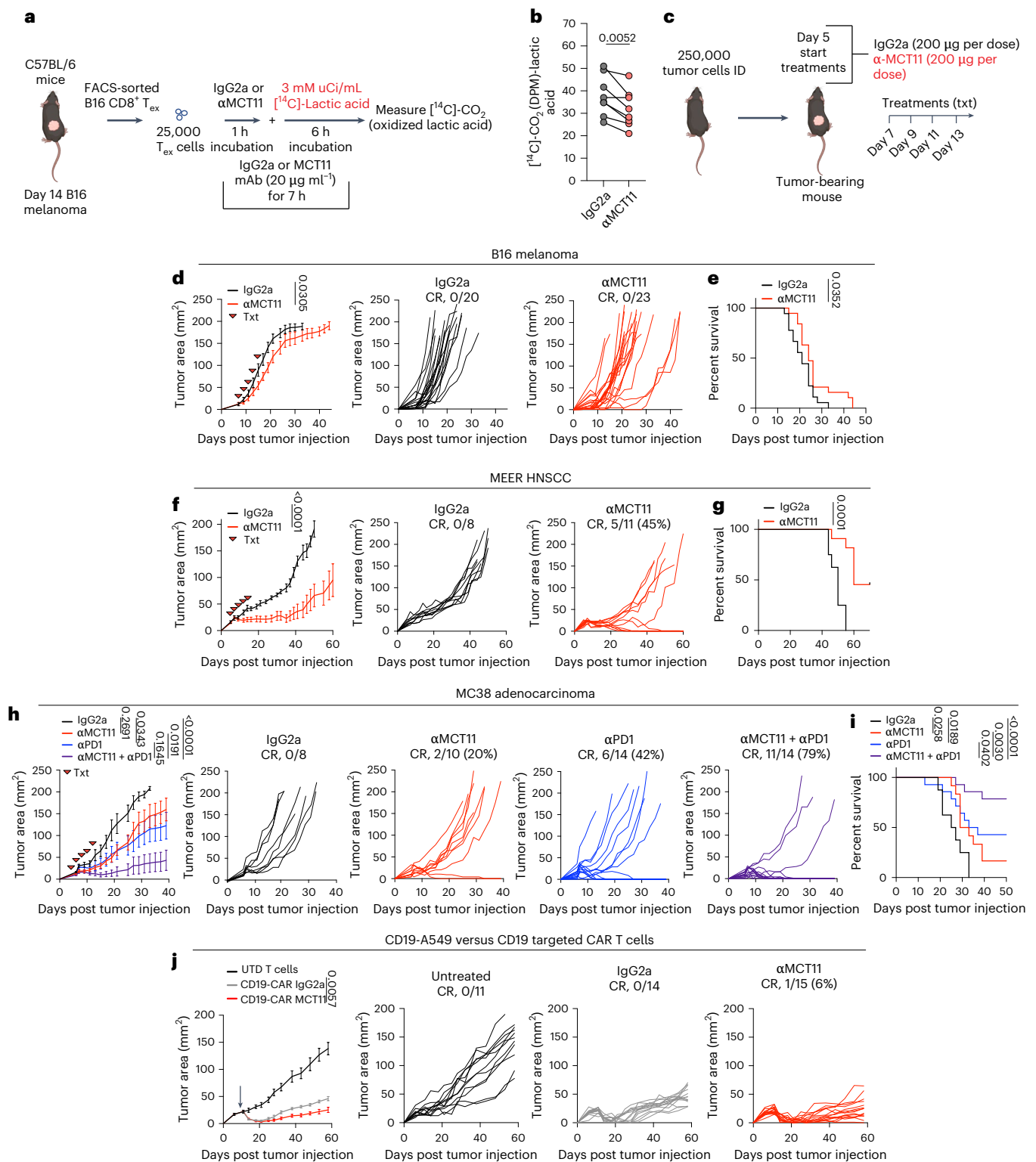


Fig. 4 | MCT11 antibody blockade reduces tumor burden in mice. **a**, T_{ex} cells were sorted from B16 melanoma tumors and cultured at 25,000 cells per well in the presence of 20 µg ml⁻¹ of IgG2a or αMCT11 for 1 h before the addition of 3 mM [¹⁴C]-lactic acid for 6 h (assay total, 7 h). **b**, Ex vivo [¹⁴C]-lactic acid oxidation in tumor-infiltrating T_{ex} cells in the presence of αMCT11 or isotype control (*n* = 8). **c**, An experimental outline for tumor growth curves with tumor cell lines, where mice were injected with 250,000 tumor cells intradermally (ID) and treated (txt) with αMCT11 or isotype control (200 µg per dose, five doses total) after day 5 of tumor growth. **d–g**, The tumor growth curves and survival curves of B16 (**d** and **e**, respectively) and MEER-bearing C57BL/6 (**f** and **g**, respectively) mice treated with αMCT11 therapy. **h, i**, Tumor growth (**h**) and survival (**i**) curve of mice injected ID

with 250,000 MC38 cells and treated with isotype control, αMCT11, αPD1 or combination therapy (200 µg per dose, five doses total). **j**, A tumor growth curve of CD19-A549-bearing NSG mice adoptively transferred with untransduced T cells (UTD) or CD19-targeting CAR-T cells treated with αMCT11 or isotype control (200 µg per dose, 12 doses total). The data represent two independent experiments for **j**, three for **d–i** or four for **b**. The error bars indicate the mean ± the standard error of the mean. The statistical analysis was performed by a paired two-tailed Student's *t*-test for **b**, by a two-way ANOVA with Tukey's multiple comparison for **d, f, h** and **j** or by a log rank Mendel–Cox test for **e, g** and **i**. Panels **a** and **c** were created with BioRender.com.

While we found no difference in the percentage of the T_{ex} population (Fig. 3e), we found T_{ex} cells lacking MCT11 (GFP⁺ cells) had a significant decrease in the per-cell expression of Tim3 (Fig. 3f) and a similar trend in PD1 expression (Fig. 3g). Further, we found improved T cell functionality upon MCT11 deletion, as T_{ex} cells from *Slc16a11*^{fl/fl}CD4^{cre} mice displayed increased polyfunctionality, by production of TNF and IFN γ , as well as increased production of IL-2 upon restimulation with α CD3/ α CD28 (Fig. 3h,i). MCT11's substrate, lactic acid, is most highly enriched in hypoxic tumor niches. Thus, we asked whether MCT11 facilitated persistence of T_{ex} cells in hypoxic niches of the tumor. Infusion of mice with pimonidazole revealed that T_{ex} cells from *Slc16a11*^{fl/fl}CD4^{cre} experienced less hypoxia than T_{ex} cells from littermate controls, while no difference was observed in T_{pe} (Fig. 3j). These data suggest MCT11-mediated lactate uptake may support T_{ex} cell accumulation in hypoxic regions, such that its deletion results in T_{ex} cells residing in more oxygenated regions where their effector functions are improved.

RNA sequencing (RNA-seq) on MCT11-deficient T_{ex} cells revealed increased expression of genes associated with T_{pe} cells (for example, *Myb*, *Cd83* and *Bcl6*) and decreased expression of genes associated with the terminal exhausted fate (for example, *Eomes*, *Havcr2*, *Id2* and *Ccl3*) (Fig. 3k). Performing a pathway enrichment analysis comparing *Slc16a11*^{fl/fl}CD4^{cre} to WT T_{ex} cells confirmed that T_{ex} cells lacking functional MCT11 harbored a transcriptome enriched for T_{pe} genes (Fig. 3l). These data suggested that T_{ex} cells from *Slc16a11*^{fl/fl}CD4^{cre} mice would be primed for a superior response to α PD1 therapy. While B16-bearing *Slc16a11*^{fl/fl}CD4^{cre} mice treated with isotype control did not grow significantly slower in comparison with WT controls (Fig. 3m), when treated with α PD1, conditional deletion of MCT11 led to 66% (4/6) complete responders (CRs), compared with only 16% CRs (1/6) in WT controls (Fig. 3n). These data suggest a metabolite flux via MCT11 promotes effector dysfunction in exhausted tumor-infiltrating CD8⁺ T cells and that it could be targeted to promote CD8⁺ T cell-mediated antitumor immunity.

MCT11 antibody blockade reduces tumor burden in mice

Immune checkpoint blockade (ICB) therapies targeting PD1, CTLA4 and LAG3 on CD8⁺ TIL has proven to be a particularly effective modality of cancer treatment³⁹. These agents act by altering signaling of T cells by preventing binding to their ligands. Given the inhibitory effect of lactic acid on T_{ex} cell function and the expression pattern on T_{ex} cells, we asked whether a monoclonal antibody against MCT11 may block lactic acid uptake in T_{ex} and promote antitumor immunity. To this end, we repeated the [¹⁴C]-lactate oxidation assay with sorted T_{ex} cells but in the presence of a monoclonal antibody targeting MCT11 (mIgG2a isotype) (Fig. 4a). Pretreatment with α MCT11 reduced the oxidation of [¹⁴C]-lactate in T_{ex} cells from B16 (Fig. 4b). As endogenous MCT11 deletion in T_{ex} cells resulted in superior T cell function (Fig. 3e,f), we treated tumor-bearing mice with α MCT11 therapeutically (Fig. 4c). α MCT11 resulted in a modest but significant decrease in tumor size in B16 melanoma-bearing mice and extension of survival without any CRs, similar to the effects of α PD1 in this model (Fig. 4d,e). However, we found striking single-agent activity in response to MCT11 blockade in MEER, where α MCT11 resulted in CRs in 45% of MEER-bearing mice (Fig. 4f,g). The MCT11 blockade required the presence of an adaptive immune response, as α MCT11 had no effect in *Rag*-deficient mice (Fig. 4h–k) and also suggested α MCT11 therapy's effect was not due to blockade of MCT11 on B16 or MEER tumor cells themselves. As the α MCT11 mAb is a murine IgG2a isotype, one potential mechanism of therapeutic efficacy may be depletion of MCT11-expressing T_{ex} cells. We, thus, generated mIgG2a α MCT11 with a LALAPG mutation, preventing FcR binding and antibody dependent cellular cytotoxicity⁴⁰. Treatment of MEER-bearing mice with the LALAPG mutant α MCT11 controlled tumor growth to the same extent as parental α MCT11 mAb (Fig. 4l,m), suggesting α MCT11 therapy functioned via a blockade. Rechallenging MCT11 blockade CRs after 1 month, in the absence of any additional

therapy, resulted in tumor clearance, suggesting the MCT11 blockade resulted in the formation of immunologic memory (Fig. 4n,o). We also tested the effects of α MCT11 in MC38, an α PD1-responsive tumor model. We found that α MCT11 alone led to CRs in MC38, with 20% of mice treated with the antibody clearing tumors (Fig. 4p). In addition, combination therapy of α MCT11 and α PD1 nearly doubled the CR rate of α PD1 therapy alone, from 42% CR in the α PD1 alone therapy to 79% in combination (Fig. 4q).

Given the differences in responses to α MCT11 therapy, we hypothesized that perhaps B16, MC38 and MEER produce metabolically distinct TMEs and, specifically, that MEER would be more lactate rich. To this end, we measured the concentration of lactic acid in the tumor interstitial fluid of B16, MC38 and MEER and found that MEER had significantly elevated levels of lactate in comparison with B16 and MC38 (Extended Data Fig. 8i). However, this did not prove that blockade of MCT11-mediated lactate metabolism provided a therapeutic benefit, as MCTs can transport other substrates, such as pyruvate, succinate, acetate, ketone bodies and other monocarboxylates⁴¹. To determine whether MCT11-targeted therapy was dependent on lactate metabolism, we performed a clustered regularly interspaced short palindromic repeats (CRISPR) with CRISPR-associated protein 9 (Cas9) knockout of the glycolytic gene *Ldha* in MEER (Extended Data Fig. 8j). Indeed, LDHA-deficient MEER cells were incapable of performing extracellular acidification after glucose and oligomycin treatment (Extended Data Fig. 8k–m). We then implanted mice with mock-knockout or LDHA-knockout MEER tumors and treated with either α MCT11 therapy or isotype control, revealing treatment with α MCT11 had no therapeutic benefit in mice bearing LDHA-deficient MEER (Extended Data Fig. 8n,o). These data suggest MCT11 therapy's efficacy is dependent on the presence of a lactate-rich TME.

Further, we asked whether MCT11 blockade could provide a therapeutic benefit for human T cells. To do this, we used a humanized chimeric antigen receptor (CAR)-T cell model system of solid tumors: CD19-expressing A549 lung cancer cells and CD19-targeting (FMC63-BBz) CAR-T cells. We implanted NOD.Cg-Prkdc^{scid}Il2rg^{tm1wjl}/SzJ (NSG) mice with 5×10^6 CD19-A549 cells and then adoptively transferred 3×10^6 CD19-CAR-T cells after 10 days of tumor growth. We then treated them with α MCT11 or isotype control twice per week until the endpoint. While both CAR-T-treated groups initially induced tumor regression, mice receiving concomitant MCT11 blockade had improved long-term tumor control (Fig. 4j). Thus, MCT11 blockade can also functionally improve human T_{ex} cells.

MCT11 blockade promotes CD8⁺ T cell antitumor immunity

We next tested the acute effects of lactic acid on T_{ex} cells during stimulation. Using our in vitro assay of continuous TCR stimulation and hypoxia, we generated T_{ex} -like cells, which express MCT11 (Extended Data Fig. 6). These cells were then restimulated in media supplemented with 0 mM or 5 mM lactic acid, with or without MCT11 antibody, for 5 h. As previously described, T cells that are continuously stimulated have reduced effector cytokine production when compared with acutely activated T cells after restimulation. The addition of 5 mM lactic acid during restimulation resulted in a reduction of TNF⁺IL-2⁺ T cells. A blockade of MCT11 during restimulation with anti-MCT11 antibody led to significantly increased percentage of polyfunctional TNF⁺IL-2⁺-producing T cells (Extended Data Fig. 6e), suggesting blockade of MCT11 desensitizes T cells of the extracellular lactate capable of acutely affecting T cell responses.

To further understand effects of α MCT11 antibody blockade on T_{ex} cells in vivo, tumor-bearing mice were treated with three doses of α MCT11 therapy, and tumor infiltrates were analyzed on day 14 (200 μ g per dose) (Fig. 5a). MCT11 blockade led to minimal changes in CD8⁺ T cell infiltration (Extended Data Fig. 9a,b), coinhibitory marker expression and cytokine production in B16 tumor infiltrates

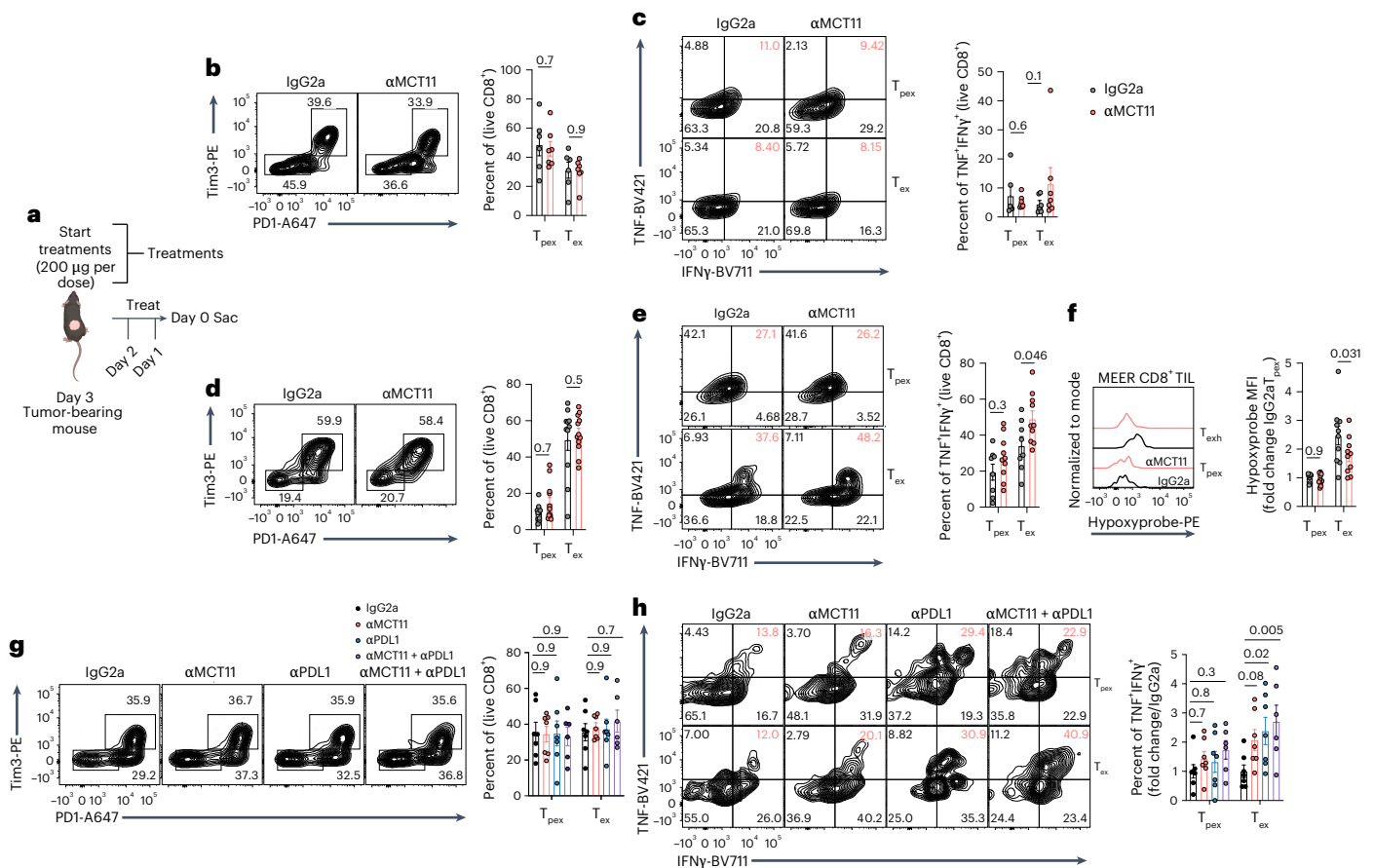


Fig. 5 | MCT11 therapy selectively enhances the polyfunctionality of T_{ex} cells.

a, A total of 250,000 tumor cells were intradermally implanted into C57BL/6 mice and treated for three consecutive days with 200 μ g per dose of α MCT11 or isotype control before sacrifice. **b**, A representative flow cytometry plot and quantification of T_{pex} and T_{ex} populations in B16 when treated with isotype control ($n = 6$) or α MCT11 ($n = 7$). **c**, A representative flow cytometry plot and quantification of TNF and IFN γ in B16 T_{pex} and T_{ex} cells after 5 h of stimulus with α CD3 (3 μ g ml⁻¹) and α CD28 (2 μ g ml⁻¹) (isotype, $n = 6$; α MCT11, $n = 7$). **d**, A representative flow cytometry plot and quantification of PD1 and Tim3 populations staining in MEER-infiltrating T_{pex} and T_{ex} cells after antibody treatment (both groups, $n = 11$). **e**, A representative flow cytometry and quantification of TNF and IFN γ in MEER-infiltrating T_{pex} and T_{ex} cells after 5 h of stimulus with α CD3 (3 μ g ml⁻¹) and α CD28 (2 μ g ml⁻¹) (both groups, $n = 11$).

f, A representative histogram and quantification of hypoxyprobe in T_{pex} and T_{ex} cells from MEER tumors after antibody treatment (isotype, $n = 10$; α MCT11, $n = 10$). **g**, A representative flow cytometry plot and quantification of PD1 and Tim3 populations staining in MC38-infiltrating CD8⁺ T cells after antibody treatment (isotype, $n = 7$; α MCT11, $n = 7$; α PDL1, $n = 7$; combo, $n = 6$). **h**, A representative cytogram and quantification of TNF and IFN γ in MC38-infiltrating T_{pex} and T_{ex} cells after 5 h of stimulus with α CD3 (3 μ g ml⁻¹) and α CD28 (2 μ g ml⁻¹) (isotype, $n = 7$; α MCT11, $n = 7$; α PDL1, $n = 7$; combo, $n = 6$). The data represent three independent experiments. The error bars indicate the mean \pm the standard error of the mean. The statistical analysis was performed by a two-way ANOVA with Sidak's multiple comparison for **b–f** or by a two-way ANOVA with Dunnett's multiple comparison test for **g** and **h**. Panel **a** was created with BioRender.com.

(Fig. 5b,c), which was not surprising given the relatively minor effect of α MCT11 therapy on B16 tumor burden. We then examined the infiltrate in MEER, given its particularly robust response to MCT11 blockade, at a timepoint before the tumor sizes diverged. The blockade of MCT11 in MEER-bearing mice resulted in increased total CD8⁺ T cells infiltrating the tumor (Extended Data Fig. 9c,d), no numerical change in the CD8⁺ TIL subpopulations (Fig. 5d) and increased CD8⁺ polyfunctionality specifically in the exhausted subpopulation (Fig. 5e). Similar to MCT11 conditional knockout animals, we found that MCT11 therapy in MEER tumors led to a decrease in hypoxia experienced by T_{ex} cells, while not affecting T_{pex} , suggesting that MCT11 blockade can redirect T_{ex} cells to nonhypoxic regions of tumors (Fig. 5f). Finally, we wanted to test the effect of α MCT11/ α PDL1 combination therapy on MC38-infiltrating CD8⁺ T cells. While no effect was observed on the number of total or subset infiltrating CD8⁺ TIL (Extended Data Fig. 9e,f and Fig. 5g), we observed selective increases in T_{ex} cell polyfunctionality (Fig. 5h). Taken together, these data suggest blockade of MCT11 on T_{ex} cells alters their function to support superior antitumor immune responses.

Discussion

Effective treatment of cancer with immunotherapy can be limited by the cellular and metabolic makeup of the TME. T cell exhaustion, a persistent dysfunctional fate acquired through altered signals and metabolic stress, renders CD8⁺ T cells unable to respond to stimulation effectively. Studies from our group and others implicate metabolic and mitochondrial dysfunction as major drivers of differentiation to the dysfunctional state of T_{ex} cells^{8,9,18,42}. However, how the metabolic microenvironment may actively enforce dysfunction in these cells remains unclear.

Our data highlight MCT11 as a novel transporter expressed on the surface of T_{ex} cells (Fig. 1). We show *Slc16a11* is poised for transcription in T_{ex} cells and is driven to expression by tissue specific factors such as hypoxia (Fig. 2). The *Slc16a11* gene locus is bound and activated by TOX and BATF (Fig. 2e,f) and that deletion of HIF1 α reduces the expression of MCT11 (Fig. 2l). It is possible other transcription factors are involved in driving the expression of MCT11 in T_{ex} cells. Commitment to exhaustion is a complex process involving large networks of TFs, such as T-bet, eomesodermin, Blimp1 and NFAT^{43–45}. Therefore, in addition to TOX and

BATF, several other TFs associated with exhaustion could be involved in driving MCT11 expression, although we suspect TFs promoted by tissue cues may be dominant in stabilizing MCT11 expression.

We also show MCT11 expression sensitizes T_{ex} cells to the TME, promoting the influx of lactic acid in tumor-infiltrating T_{ex} cells, limiting their effector functions (Fig. 3). Notably, conditional deletion of MCT11 in T_{ex} cells reduced lactic acid metabolism nearly to the level of T_{pex} cells (Fig. 1m). This caused the retention of a progenitor-like transcriptional program in T_{ex} cells, with increased *Tcf7* and *Myb* expression, TFs shown to promote response to α PD1 therapy^{4,46}. Therefore, MCT11 deficient mice were primed for a superior response to α PD1 therapy (Fig. 3h–k).

T_{ex} cells are characterized by upregulating multiple coinhibitory receptors, but these cells also express high levels of costimulatory molecules, cytokine receptors and, as we've demonstrated here, a unique set of nutrient transporters. While ICBs have been a groundbreaking success in the clinic, only ~20% of patients with cancer respond to immunotherapy⁴⁷. Identifying new targets for immunotherapy has been a challenge due to redundancy in checkpoint receptors and potential autoimmune side effects blocking inhibitory pathways. Importantly, MCT11 blockade acts on a distinct pathway than traditional ICBs, as MCT11 blockade interferes with a metabolic process as opposed to blocking the repression of T cell activation. MCT11 antibody blockade has an effect as a monotherapy, leading to complete responses in MC38 and MEER models and also as a combination therapy, doubling the CRs in mice bearing MC38 tumors in combination with α PD1 (Fig. 4e,f). MCT11 offers an exciting novel target given its unique expression in tumor-infiltrating PD1^{hi} and T_{ex} CD8⁺ T cells (Fig. 1l and Extended Data Fig. 4). Further, according to the NCBI tissues gene atlas, MCT11 expression is limited (mean RPKM of ~1) and restricted to small populations of cells in the liver, lung and kidney. Short-term targeting of MCT11 in patients with cancer could, thus, limit the possibilities of potential toxicities and adverse autoimmune reactions. Supporting this is that a germline-knockout mouse²⁸ and our own pan-tissue conditional knockout animal have no overt phenotypes.

Lactic acid has long been associated with immunosuppression, and we and others have discussed how lactic acid buildup in cancer can promote an environment of immunosuppression by directly inhibiting T cells^{12,13} and by stabilizing regulatory T cells³⁰. However, lactate may not be universally suppressive; recent studies have shown that lactate is an essential carbon source for the TCA cycle in CD8⁺ T cells⁴⁸. Nevertheless, concentration is important, and lactic acid is present at up to ten times higher in the TME than in serum³¹. In addition, lactic acid extruded by cancer cells acidifies the TME, which can have inhibitory effects on CD8⁺ T cell antigen recognition, cytokine production and cytotoxicity^{12,13}. While T cells utilize lactate to fuel the TCA cycle, hypoxia reduces the ability to engage OXPHOS, and it is possible that a large influx of monocarboxylates through MCT11 could lead to inefficient buildup and storage of carbon, stabilization of lactate-sensitive transcription factors or alterations to the epigenome. In support of this idea, a recent study showed that tumor-infiltrating CD8⁺ T cells had an increase in intracellular accumulation of lactic acid, which was not being efficiently shuttled into the mitochondria and led to increased histone lysine lactylation⁴⁹. Further, signals such as persistent TCR stimulation, inflammation and checkpoint receptor signaling may alter the ways in which lactate may be metabolized by cells. Further, while this study focuses on lactic acid, we do not discount other monocarboxylates present in the TME, albeit at much lower concentrations than lactic acid, as substrates for MCT11. Members of the MCT family can transport multiple monocarboxylates⁴¹ such as pyruvate²⁷, acetate, succinate and ketone bodies.

Our study supports an evolving model of CD8⁺ T_{ex} cells being essentially hypersensitive to their extracellular milieu, both in costimulatory/inhibitory receptors and also nutrients. They upregulate MCT11, which renders them sensitive to lactic acid present at high levels in the TME. Teleologically, MCT11 may be expressed in CD8⁺ T cells to export lactic acid inside of highly metabolically active cells, or it may have evolved to

allow tissues (which can accumulate lactate as a consequence of inflammation) to shape inflammatory function in persistently stimulated T cells. Our study highlights how immunity can be shaped by the local metabolic environment, such that over the course of differentiation, cells dynamically alter their nutrient transporter expression, rendering them differentially sensitive to metabolites in various tissues. By modulating nutrient transporters, such as in the case of MCT11, terminally differentiated T cells can be rendered insensitive to metabolites such as lactic acid, driving tumor eradication and therapeutic response.

Online content

Any methods, additional references, Nature Portfolio reporting summaries, source data, extended data, supplementary information, acknowledgements, peer review information; details of author contributions and competing interests; and statements of data and code availability are available at <https://doi.org/10.1038/s41590-024-01999-3>.

References

- Zhang, N. & Bevan, J. Michael. CD8⁺ T cells: foot soldiers of the immune system. *Immunity* **35**, 161–168 (2011).
- Ando, M., Ito, M., Srirat, T., Kondo, T. & Yoshimura, A. Memory T cell, exhaustion, and tumor immunity. *Immunol. Med.* **43**, 1–9 (2020).
- Mclane, L. M., Abdel-Hakeem, M. S. & Wherry, E. J. CD8 T cell exhaustion during chronic viral infection and cancer. *Annu. Rev. Immunol.* **37**, 457–495 (2019).
- Miller, B. C. et al. Subsets of exhausted CD8⁺ T cells differentially mediate tumor control and respond to checkpoint blockade. *Nat. Immunol.* **20**, 326–336 (2019).
- Siddiqui, I. et al. Intratumoral Tcf1⁺PD-1⁺CD8⁺ T cells with stem-like properties promote tumor control in response to vaccination and checkpoint blockade immunotherapy. *Immunity* **50**, 195–211.e110 (2019).
- Zhao, S., Peralta, R. M., Avina-Ochoa, N., Delgoffe, G. M. & Kaech, S. M. Metabolic regulation of T cells in the tumor microenvironment by nutrient availability and diet. *Semin. Immunol.* **52**, 101485 (2021).
- Multhoff, G., Radons, J. & Vaupel, P. Critical role of aberrant angiogenesis in the development of tumor hypoxia and associated radioresistance. *Cancers* **6**, 813–828 (2014).
- Scharping, N. E. et al. Mitochondrial stress induced by continuous stimulation under hypoxia rapidly drives T cell exhaustion. *Nat. Immunol.* <https://doi.org/10.1038/s41590-020-00834-9> (2021).
- Liu, Y.-N. et al. Hypoxia induces mitochondrial defect that promotes T cell exhaustion in tumor microenvironment through MYC-regulated pathways. *Front. Immunol.* <https://doi.org/10.3389/fimmu.2020.01906> (2020).
- Chang, C.-H. et al. Metabolic competition in the tumor microenvironment is a driver of cancer progression. *Cell* **162**, 1229–1241 (2015).
- De La Cruz-López, K. G., Castro-Muñoz, L. J., Reyes-Hernández, D. O., García-Carrancá, A. & Manzo-Merino, J. Lactate in the regulation of tumor microenvironment and therapeutic approaches. *Front. Oncol.* <https://doi.org/10.3389/fonc.2019.01143> (2019).
- Fischer, K. et al. Inhibitory effect of tumor cell-derived lactic acid on human T cells. *Blood* **109**, 3812–3819 (2007).
- Mendler, A. N. et al. Tumor lactic acidosis suppresses CTL function by inhibition of p38 and JNK/c-Jun activation. *Int. J. Cancer* **131**, 633–640 (2012).
- Stine, Z. E., Schug, Z. T., Salvino, J. M. & Dang, C. V. Targeting cancer metabolism in the era of precision oncology. *Nat. Rev. Drug Discov.* **21**, 141–162 (2022).
- Pizzagalli, M. D., Bensimon, A. & Superti-Furga, G. A guide to plasma membrane solute carrier proteins. *FEBS J.* **288**, 2784–2835 (2021).

16. Belouèche-Babari, M. et al. Monocarboxylate transporter 1 blockade with AZD3965 inhibits lipid biosynthesis and increases tumour immune cell infiltration. *Br. J. Cancer* **122**, 895–903 (2020).
17. Bian, Y. et al. Cancer SLC43A2 alters T cell methionine metabolism and histone methylation. *Nature* **585**, 277–282 (2020).
18. Scharping, N. E. et al. The tumor microenvironment represses T cell mitochondrial biogenesis to drive intratumoral T cell metabolic insufficiency and dysfunction. *Immunity* **45**, 374–388 (2016).
19. Najjar, Y. G. et al. Tumor cell oxidative metabolism as a barrier to PD-1 blockade immunotherapy in melanoma. *JCI Insight* <https://doi.org/10.1172/jci.insight.124989> (2019).
20. Lin, L., Yee, S. W., Kim, R. B. & Giacomini, K. M. SLC transporters as therapeutic targets: emerging opportunities. *Nat. Rev. Drug Discov.* **14**, 543–560 (2015).
21. Ford, B. R. et al. Tumor microenvironmental signals reshape chromatin landscapes to limit the functional potential of exhausted T cells. *Sci. Immunol.* **7**, eaj9123 (2022).
22. Ruffin, A. T. et al. B cell signatures and tertiary lymphoid structures contribute to outcome in head and neck squamous cell carcinoma. *Nat. Commun.* <https://doi.org/10.1038/s41467-021-23355-x> (2021).
23. Cillo, A. R. et al. Immune landscape of viral- and carcinogen-driven head and neck cancer. *Immunity* **52**, 183–199.e189 (2020).
24. Zheng, L. et al. Pan-cancer single-cell landscape of tumor-infiltrating T cells. *Science* <https://doi.org/10.1126/science.abe6474> (2021).
25. Halestrap, A. P. The monocarboxylate transporter family—structure and functional characterization. *IUBMB Life* **64**, 1–9 (2012).
26. Consortium, T. S. T. D. G. Sequence variants in SLC16A11 are a common risk factor for type 2 diabetes in Mexico. *Nature* **506**, 97–101 (2014).
27. Rusu, V. et al. Type 2 diabetes variants disrupt function of SLC16A11 through two distinct mechanisms. *Cell* **170**, 199–212.e120 (2017).
28. Zhao, Y. et al. Gain-of-function mutations of SLC16A11 contribute to the pathogenesis of type 2 diabetes. *Cell Rep.* **26**, 884–892.e884 (2019).
29. Chen, Y. et al. CD147 regulates antitumor CD8⁺ T cell responses to facilitate tumor-immune escape. *Cell. Mol. Immunol.* **18**, 1995–2009 (2021).
30. Watson, M. J. et al. Metabolic support of tumour-infiltrating regulatory T cells by lactic acid. *Nature* **591**, 645–651 (2021).
31. Parks, S. K., Mueller-Klieser, W. & Pouyssegur, J. Lactate and acidity in the cancer microenvironment. *Annu. Rev. Cancer Biol.* **4**, 141–158 (2020).
32. Economides, A. N. et al. Conditionals by inversion provide a universal method for the generation of conditional alleles. *Proc. Natl Acad. Sci. USA* **110**, E3179–E3188 (2013).
33. Zhang, Z. Cre recombinase-mediated inversion using lox66 and lox71: method to introduce conditional point mutations into the CREB-binding protein. *Nucleic Acids Res.* **30**, 90e (2002).
34. Eliasson, P. & Jönsson, J.-I. The hematopoietic stem cell niche: low in oxygen but a nice place to be. *J. Cell. Physiol.* **222**, 17–22 (2010).
35. Petrova, V., Annicchiarico-Petruzzelli, M., Melino, G. & Amelio, I. The hypoxic tumour microenvironment. *Oncogenesis* <https://doi.org/10.1038/s41389-017-0011-9> (2018).
36. Kim, A.-R. et al. Spatial immune heterogeneity of hypoxia-induced exhausted features in high-grade glioma. *Oncol Immunology* <https://doi.org/10.1080/2162402x.2022.2026019> (2022).
37. Sattiraju, A. et al. Hypoxic niches attract and sequester tumor-associated macrophages and cytotoxic T cells and reprogram them for immunosuppression. *Immunity* **56**, 1825–1843.e1826 (2023).
38. Aguilera, K. & Brekken, R. Hypoxia studies with pimonidazole in vivo. *Bio Protoc.* **4**, e1254 (2014).
39. Esfahani, K. et al. A review of cancer immunotherapy: from the past, to the present, to the future. *Curr. Oncol.* **27**, 87–97 (2020).
40. Lo Nigro, C. et al. NK-mediated antibody-dependent cell-mediated cytotoxicity in solid tumors: biological evidence and clinical perspectives. *Ann. Transl. Med.* **7**, 105 (2019).
41. Bosshart, P. D., Charles, R.-P., Garibsingh, R.-A., Schlessinger, A. & Fotiadis, D. SLC16 family: from atomic structure to human disease. *Trends Biochem. Sci.* **46**, 28–40 (2021).
42. Vardhana, S. A. et al. Impaired mitochondrial oxidative phosphorylation limits the self-renewal of T cells exposed to persistent antigen. *Nat. Immunol.* **21**, 1022–1033 (2020).
43. Shin, H. et al. A role for the transcriptional repressor Blimp-1 in CD8⁺ T cell exhaustion during chronic viral infection. *Immunity* **31**, 309–320 (2009).
44. Paley, M. A. et al. Progenitor and terminal subsets of CD8⁺ T cells cooperate to contain chronic viral infection. *Science* **338**, 1220–1225 (2012).
45. Martinez, G. J. et al. The transcription factor NFAT promotes exhaustion of activated CD8⁺ T cells. *Immunity* **42**, 265–278 (2015).
46. Tsui, C. et al. MYB orchestrates T cell exhaustion and response to checkpoint inhibition. *Nature* **609**, 354–360 (2022).
47. Ribas, A. & Wolchok, J. D. Cancer immunotherapy using checkpoint blockade. *Science* **359**, 1350–1355 (2018).
48. Kaymak, I. et al. Carbon source availability drives nutrient utilization in CD8⁺ T cells. *Cell Metab.* **34**, 1298–1311 (2022).
49. Ma, J. et al. Lithium carbonate revitalizes tumor-reactive CD8⁺ T cells by shunting lactic acid into mitochondria. *Nat. Immunol.* **25**, 552–561 (2024).

Publisher's note Springer Nature remains neutral with regard to jurisdictional claims in published maps and institutional affiliations.

Open Access This article is licensed under a Creative Commons Attribution 4.0 International License, which permits use, sharing, adaptation, distribution and reproduction in any medium or format, as long as you give appropriate credit to the original author(s) and the source, provide a link to the Creative Commons licence, and indicate if changes were made. The images or other third party material in this article are included in the article's Creative Commons licence, unless indicated otherwise in a credit line to the material. If material is not included in the article's Creative Commons licence and your intended use is not permitted by statutory regulation or exceeds the permitted use, you will need to obtain permission directly from the copyright holder. To view a copy of this licence, visit <http://creativecommons.org/licenses/by/4.0/>.

© The Author(s) 2024

Methods

Tumor cell lines

We obtained B16-F10 (CRL-6475) and A549 (CCL-185) cells from the American Type Culture Collection. We obtained MC38 (available at Kerfast) cells from D.A.A. Vignali (University of Pittsburgh) and MEER cells from R. Ferris (University of North Carolina). The B16, A549 and MC38 cell lines were authenticated via sequencing by their supplier. MEER cells were generated by overexpressing E6/E7 and Ras in primary mouse tonsil epithelial cells⁵⁰ and were probed by western blot to confirm E6/E7 and Ras overexpression. MC38 and MEER were confirmed mycoplasma free in 2016 and B16 in 2018. Primary and immortalized cell lines were maintained in laboratory-made R10 medium (RPMI 1640, 10% fetal bovine serum, 2 mM L-glutamine, penicillin plus streptomycin, nonessential amino acids, 1 mM sodium pyruvate, 5 mM HEPES buffer and β -mercaptoethanol). The cultures were incubated in temperature-stable and partial-pressure-stable conditions at 37 °C and 5% CO₂.

Mice

The work with mice was done in accordance with the Institutional Animal Care and Use Committee at the University of Pittsburgh. The mice were housed on a 12 h light–dark cycle in boxes (either four males or five females per box), in specific pathogen-free conditions. All experimental mice were fed with Purina Prolab Isopro RMH 3000 (5P75 and 5P76) chow ad libitum. Male and female mice were used on a C57BL/6 background between the ages of 8 and 12 weeks. *Slc16a1*^{fl/fl} mice were generated by S. Gingras (University of Pittsburgh). NSG, C57BL/6, SJ/L (Thy1.1), CMV^{Cre}, *Cd4*^{Cre} and Tg(TcrTcrb)1100Mjb/J (OT-I) mice were obtained from the Jackson Laboratory.

Tumor growth curves and therapies

Slc16a1^{fl/fl} or *Slc16a1*^{fl/fl} × CD4^{Cre} mice were injected with B16 100,000 cells in RPMI medium and treated with 200 μ g per dose of α PD1 (Bio X Cell; clone RMP1-14; catalog number BE0146) for three total doses. For α MCT11-treated tumor growth curves, C57BL/6 or *Rag2*-knockout mice were injected with 250,000 cells of either B16, MC38 or MEER in serum-free RPMI. Starting when tumors were palpable (day 5–7) mice were treated with 200 μ g per dose of mlgG2a isotype control (Bio X Cell), α PD1 (Bio X Cell; clone J43; catalog number BE0033-2), α MCT11 or LALAPG Fc mut α MCT11, which were administered every other day for a total of five doses. Anti-MCT11 was originally raised in mice against a human N-terminal peptide, and the monoclonal parental or LALAPG anti-MCT11 used in this study was generated recombinantly in CHO cells (Evitria). The tumors were measured three times per week using digital calipers. The maximal tumor size was reached when a tumor grew to 15 mm in size in any direction, at which point the tumor-bearing mouse was killed. The mice were excluded from analysis when tumors became ulcerated before the tumor reached maximal size.

Tumor and lymph node collection and mechanical disruption

For T cell single-cell suspension, LNs and spleens of mice were mechanically disrupted with the back end of a syringe plunger and filtered through 70 μ m filters (Fisher brand). For tumor single-cell suspensions, whole tumors were injected with 2 mg ml⁻¹ of collagenase type IV, 2 U ml⁻¹ of dispase and 10 U ml⁻¹ of DNase I (Sigma) in buffered RPMI and incubated for 20 min at 37 °C. The tumors were then mechanically disrupted using the back end of a syringe plunger and filtered through 70 μ m filters (Fisher brand).

LCMV infections

C57BL/6 mice were inoculated with LCMV clone 13 (2 × 10⁶ plaque forming units (PFU) by retro-orbital injection). The mice were monitored for weight loss to determine whether they were infected. The mice were sacrificed on day 14 post infection and their LNs, spleens, liver, kidney, lung and BM were collected. The organs were mechanically disrupted

as described above to reach a single-cell suspension. Antigen specific T_{ex} cells were identified using a gp33* tetramer gifted by Larry Kane (University of Pittsburgh).

CD8⁺ T cell negative selection

CD8⁺ T cells were purified by negative selection from LNs and tumor single-cell suspensions. These were performed using Mojosort magnetic-beads (BioLegend) and the following biotinylated antibodies (BioLegend): CD4 (RM4-5, catalog number 100508, lot number B286276, dilution 1:1,000), CD19 (6D5, catalog number 115504, lot number B353713, dilution 1:1,000), CD11c (N418, catalog number 117304, lot number B317309, dilution 1:1,000), CD11b (M1/70, catalog number 101204, lot number B307868, dilution 1:1,000), Ly6G/Ly6C (Gr-1, catalog number 108404, lot number B351067, dilution 1:1,000), TCR γ δ (GL3, catalog number 118103, lot number B355058, dilution 1:1,000), B220 (RA3-6B2, catalog number 103204, lot number B352779, dilution 1:500), CD49 (DX5, catalog number 108904, lot number B285502, dilution 1:500), CD105 (MJ7/18, catalog number 120404, lot number B266720, dilution 1:500), CD24 (M1/69, catalog number 101803, lot number B360781, dilution 1:500) and CD16/32 (93, catalog number 101303, lot number B355428, dilution 1:500).

Hypoxia detection with pimonidazole

For experiments using Hypoxyprobe, the mice were retro-orbitally injected with pimonidazole (80 mg kg⁻¹, Hypoxyprobe) in PBS 1 h before they were killed. Pimonidazole was detected using antipimonidazole antibodies (Hypoxyprobe) after 10 min of 4% paraformaldehyde (PFA) fixation, followed by Foxp3 Fix/Perm permeabilization for 20 min.

Flow sorting and cytometry

For extracellular stains, the samples were incubated on ice for 20 min in an antibody cocktail mix. For intracellular stains, the samples were incubated on ice for 20 min in an antibody cocktail mix after fixation. The antibodies were obtained from the following companies: BioLegend: anti-CD4 (GK1.5, catalog number 100412, lot number B184560, dilution 1:1,000), anti-CD8 (53-6.7, catalog number 100707, lot number B171971, dilution 1:1,000), anti-CD44 (IM7, catalog number 103032, lot number B267976, dilution 1:500), CD45 (I3/2.3, catalog number 147711, lot number B254856, dilution 1:1,000) anti-CD147 (OX-114, catalog number 123716, lot number B262975, dilution 1:500), anti-CD19 (6D5, catalog number 115530, lot number B276004, dilution 1:1,000), anti-Ly6G (1A8, catalog number 127616, lot number B248844, dilution 1:500), anti-Ly6C (HK1.4, catalog number 128017, lot number B213757, dilution 1:500), anti-MHCII (M5/114.15.2, catalog number 107612, lot number B251993, dilution 1:500), anti-F4 80 (BM8, catalog number 123149, lot number B326894, dilution 1:250), anti-CD279 (PDI, 29F.1A12, catalog number 135221, lot number B194160, dilution 1:250), anti-HAVcr-2 (TIM3, RMT3-23, catalog number 119705, lot number B224472, dilution 1:250), anti-IFN γ (XMG1.2, catalog number 505842, lot number B270630, dilution 1:250), anti-TNF (MP6-XT22, catalog number 506322, lot number B218553, dilution 1:500), anti-CD11b (M1/70, catalog number 101204, lot number B307868, dilution 1:250) and anti-CD11c (N418, catalog number 117320, lot number B286499, dilution 1:250); Invitrogen: anti-CD62L (MEL-14, catalog number 564109, lot number 7341887, dilution 1:500), and anti-TOX (TXRX10, catalog number 80-6502-82, lot number 2246902, dilution 1:250). The human samples were stained with the following antibodies (BioLegend): anti-PDI (EH12.2Z7, catalog number 329904, dilution 1:200), anti-TIM3 (F382E2, catalog number 345006, dilution 1:200), anti-CD8 (HIT8a, catalog number 300918, dilution 1:200) and anti-CD3 (SK7, catalog number 344834, dilution 1:200). For panels targeting transcription factors, the cells were fixed with the Foxp3 fix/perm buffer set (BioLegend) according to the manufacturer's protocol. For panels targeting cytokines, fixation was performed with Cytotfix/Cytoperm (BD Biosciences) according to the manufacturer's protocol. The data collection utilized BD FACSDiva v9.0 for flow cytometry and was analyzed via FlowjoV10.

CD8⁺ TIL cytokine production assay

Tumor and lymph node cell suspensions were stimulated in complete R10 medium with Golgi-Plug (BD Biosciences), 3 $\mu\text{g ml}^{-1}$ plate-bound αCD3 and 2 $\mu\text{g ml}^{-1}$ αCD28 in complete R10 medium with Golgi-Plug for 5 h at 37 °C. In addition, dLNs and tumor cells were cultured in complete R10 medium Golgi-Plug, as a no stimulus control to determine gating strategies.

CRISPR–Cas9 knockout

The CRISPR–Cas9-mediated knockout method was modified on the basis of a previous publication. A total of 10 μg of Alt-R S.p. Cas9 Nuclease V3 (IDT) was mixed with an LDHa-targeted sgRNA (AAGCTGGTCATATACCGC) to form an RNP complex. A total of 2 million MEER cells were mixed with the RNP and Lonza SF buffer along with the Alt-R Cas9 Electroporation Enhancer for electroporation. The DJ-110 program (Lonza 4D Nucleofector) was used for electroporation.

Tumor interstitial fluid lactate measurement

The tumors were collected from mice and measured for tumor weight. The tumors were then cut up and placed on 20 mm nylon filters (Spectrum labs) and placed in top of 50 ml conical tube, wedged between the cap and the filter. The conical tube was then spun for 5 min at 2,000g. Approximately 20 μl of tumor interstitial fluid was then collected from the bottom of the conical tube. To measure lactate concentrations, we utilized a lactate meter (Nova Biomedical). The lactate concentration was then divided by tumor weight to generate final concentration of lactate.

T cell transduction, retroviral overexpression of MCT11 and adoptive transfer

The *Slc16a11* murine coding sequence was obtained from the National Institutes of Health (NIH) database and cloned via Gibson assembly into a murine stem cell virus retroviral expression vector, which also encodes for an internal ribosome entry site–mCherry cassette. The vector was transfected into the Plat-E retroviral packaging cell line. The CD8⁺ T cells were collected and negatively isolated with Mojo beads (as described above) and were stimulated for 24 h with 5 $\mu\text{g ml}^{-1}$ of αCD3 , 2 $\mu\text{g ml}^{-1}$ of αCD28 and 50 U ml^{-1} of IL-2. After 48 h, Plat-E retroviral supernatant was collected and supplemented with 5 $\mu\text{g ml}^{-1}$ polybrene. The OT-IT cells were spun down and transduced in the viral supernatant for 2 h at 2,000 rpm. The cells were expanded and sorted via mCherry fluorescence on day 3 post transduction. A total of 3×10^6 OT-I T cells were then retro-orbitally transferred into D7 B16^{OVA}-bearing mice.

Human CAR-T cell production and adoptive transfer

Human CD8⁺ T cells were isolated from bulk PBMCs from the blood bank. The T cells were then stimulated with anti-CD3/CD28 Dynabeads in RPMI supplemented with 10% fetal bovine serum (v/v) and 200 U ml^{-1} human IL-2 at 37 °C with 5% CO₂ for 48 h. Then, CD19-CAR-expressing retrovirus was added to the expanding cells. After 5 days of expansion, Dynabeads were magnetically removed, and the cells were expanded for another 5 days in the presence of IL-2. CD19-A549-bearing NSG mice were adoptively transferred with 3×10^6 human CD8⁺ T cells expressing CD19-CAR.

Transcriptomic analysis by RNA-seq

RNA-seq data of B16 melanoma CD8⁺ TIL populations²¹ was utilized to evaluate expression of SLCs (GSE175408). For sequencing of the MCT11 conditional knockout T cells, 350 T_{ex} cells were sorted from B16 tumors into lysis buffer in a 96-well plate. For all samples, complementary DNA was generated using the SMARTer Ultra Low Input RNA Kit for sequencing. The libraries were generated using the Nextera XT kit (Illumina) with 1 ng of cDNA in a total of 5 μl . Sequencing was done using a P3 flow cell-NextSeq2000. Bulk RNA-seq analysis was performed on Partek-Flow. The paired-end reads were concatenated into a single fastq file.

The reads were trimmed for adapters using Cutadapt v1.12 before being aligned to *Mus musculus* reference genome (mm38) using the RNA-seq aligner STAR2.7. Using the raw counts, differential genes were found by DESeq2. Publicly available RNA-seq data²¹ from WT T_{ex} cells were used as controls (GSE175408). A gene set enrichment analyses of selected immunologic signature and hallmark gene sets was performed with clusterProfiler (<https://doi.org/10.1016/j.xinn.2021.100141>).

Transcriptomic analysis by single-cell RNA-seq

Single-cell RNA-seq data from blood and tumor-infiltrating immune populations from a cohort of patients with head and neck cancer^{22,23} was utilized to evaluate the expression of MCT11 across subsets of CD8⁺ T cells. Feature/barcode expression matrices were downloaded from the Gene Expression Omnibus (GSE139324), and cell type annotations were inferred as previously described^{3,4}. CD8⁺ T cells were then bioinformatically isolated from other immune populations, and the top 2,000 highly variable genes were used as input for dimensionality reduction with principal component analysis. The top principal components were identified heuristically by identifying the inflection point on an elbow plot and were subsequently used for generating uniform manifold approximation and projection embeddings and Louvian-based clustering. The coexpression of *PDCDI*, *HAVCR2* and *SLC16A11* was then evaluated across clusters in PBMC and TIL and was visualized with a heat map.

[¹⁴C]-lactic acid oxidation experiments

The protocol is modified from previous published research⁵¹. T cells were incubated for 6 h in 0.2 ml RPMI containing 3 mM uCi ml^{-1} [¹⁴C]-lactic acid, sodium salt (NEC599050UC, PerkinElmer) and 2.5 mM sodium lactate. Afterward, the medium was transferred to borosilicate glass tubes. Each glass tube contained a microcentrifuge tube filled with 1 N sodium hydroxide to absorb CO₂. The glass tubes were then sealed, and 5 N hydrochloric acid was injected into each tube to stop cellular metabolism and release carbon dioxide. After overnight absorption of [¹⁴C]-CO₂, the samples were analyzed by liquid scintillation counting. A total of 25,000 T cells were used for ex vivo TIL studies and 100,000 were used for MCT11 overexpressing cells.

Continuous stimulation under hypoxia assay

The protocol was previously published⁸. Briefly, CD8⁺ T cells were isolated from mouse LNs or human PBMCs. The T cells were then activated at a 1:1 ratio with CD3/CD28 Dynabeads for 24 h. After 24 h, the T cells were split into four groups: acute TCR stimulus (no beads for remainder of assay in 20% oxygen), acute TCR stimulus under hypoxia (no beads for remainder of assay in 1.5% oxygen), continuous stimulus (10:1 beads to T cells for remainder of assay in 20% oxygen) and continuous stimulus under hypoxia (10:1 beads to T cells for remainder of assay in 1.5% oxygen). The T cells were kept in those conditions for 6 days (mouse assay) or 8 days (human assay) at a 1 million per milliliter concentration in R10 media with 50 IU IL-2.

Extracellular flux analysis

In vitro cultured B16 and MEER tumor cell lines were plated on an Agilent Seahorse poly-D-lysine-coated cell culture plate at 25,000 cells per well in minimal RPMI supplemented with 2 mM glutamine. The basal glycolytic rates were measured for 30 min, following the injections of 10 mM glucose, 2 μM oligomycin and 10 mM 2-deoxyglucose, and the readings were continued for 3 h. The measurements were performed on the XFe96 Analyzer.

Western blots

The tumor cells were lysed in RIPA lysis buffer with sodium orthovanadate and protease inhibitor for 15 min on ice. The lysates were spun down via high-speed centrifugation to clear debris and samples were mixed with 4 \times lithium dodecyl sulfate (LDS) buffer and boiled

for 10 min. The lysates were loaded onto gels and ran at 200 V for 60 min. The proteins were transferred onto nitrocellulose membranes with transfer buffer at 30 V for 90 min. Blocking of the membrane was performed with nonfat dry milk for 1 h and washed with Tris-buffered saline + 0.1% Tween-20 (TBST). The membranes were washed three times with TBST and probed with a primary antibody overnight and horseradish peroxidase (HRP)-conjugated secondary antibody for 1 h at 4 °C. The membrane was then washed three times with TBST and incubated for 1 min with chemiluminescent substrate. The western blots were detected via chemiluminescent exposure to film. The antibodies used were b actin (Cell Signaling Technology) and LDHA (Cell Signaling Technology).

Sample sizes, randomization and blinding

No statistical methods were used to predetermine sample sizes, but our sample sizes are similar to those reported in previous publications. The tumor growth curves were randomized on the basis of initial tumor size once tumors became palpable, ensuring even distribution across groups. All tumor growth curves were conducted in a blinded manner—one author administered treatments while another independently measured tumor size. For all other experiments, data collection and analysis were not performed blind to the conditions of the experiments.

Statistical analysis

The data distribution was assumed to be normal, but this was not formally tested. We used unpaired or paired Student's *t*-tests, one-way analysis of variance (ANOVA) with Tukey's multiple comparisons or two-way ANOVA with Tukey's, Dunnett's or Šidák's multiple comparison tests to calculate the *P* values in GraphPad Prism. For tumor growth curves and survival curves, the *P* values were calculated using two-way ANOVA with Tukey's multiple comparison and a log rank Mendel–Cox test, respectively. Statistical tests for specific experiments can be found in the figure legends. Grubb's test was utilized to determine whether a value was a significant statistical outlier.

Reporting summary

Further information on research design is available in the Nature Portfolio Reporting Summary linked to this article.

Data availability

RNA-seq data have been deposited in the Gene Expression Omnibus (GEO) under accession code [GSE249944](https://www.ncbi.nlm.nih.gov/geo/query/acc.cgi?acc=GSE249944). Single-cell RNA-seq from the GEO repository are deposited under accession code [GSE139324](https://www.ncbi.nlm.nih.gov/geo/query/acc.cgi?acc=GSE139324). Source data for Fig. 1a,b and Extended Data Fig. 2b, as well as WT control for Fig. 3g,h, are available in the GEO repository under accession code [GSE175408](https://www.ncbi.nlm.nih.gov/geo/query/acc.cgi?acc=GSE175408).

References

- Jung, Y.-S. et al. CD200: association with cancer stem cell features and response to chemoradiation in head and neck squamous cell carcinoma. *Head Neck* **37**, 327–335 (2015).
- Chen, X., Sherman, J. W. & Wang, R. Radioisotope-based protocol for determination of central carbon metabolism in T cells. *Methods Mol. Biol.* **2111**, 257–265 (2020).

Acknowledgements

We thank all members of the Delgoffe Laboratory for constructive discussions. Trainees on this work were supported by: 1F31AI152429-01A1 and T32AI089443 for R.M.P. and 5F31CA257760 and

T32CA082084 for A.F. This work was supported by an NIH Director's New Innovator Award (DP2AI136598) the NIAID and NCI (R01AI171483, R01AI166598 and R01CA277473), the Hillman Fellows for Innovative Cancer Research Program a Stand Up to Cancer–American Association for Cancer Research innovative research grant (SU2C-AACR-IRG-04-16), the UPMC Hillman Cancer Center Skin Cancer and Head and Neck Cancer SPOREs (P50CA121973 and P50CA097190; NIH), the Mark Foundation for Cancer Research's Emerging Leader Award and a Cancer Research Institute–Lloyd J. Old STAR Award (all to G.M.D.).

Author contributions

R.M.P. designed and performed the majority of experiments, analyzed data and wrote the manuscript. B.X. performed [¹⁴C]-lactic acid oxidation experiments. H.N.R. contributed to the generation of MCT11 in T_{ex} of LCMV C13-infected mice. K.S. designed continuous stimulus and hypoxia experiments. S.J. performed some of the humanized CAR-T cell studies. A.F. and D.B.R. performed detailed statistical analysis on many figures. M.P. and V.D. measured tumors blinded and generated tumor growth curves. K.L. designed overexpression vectors. B.R.F. analyzed previously published RNA-seq and CUT&RUN data comparing T_{prex} to T_{ex} cells. K.Q. generated bubble plots of RNA-seq data comparing WT to *Slc16a11^{fl/fl}*xCD4^{Cre} mice. A.R.C. analyzed single-cell RNA-seq data. S.G. designed and generated *Slc16a11^{fl/fl}* COIN mouse. A.C.P. oversaw bioinformatics research. L.P.K. oversaw and directed research. G.M.D. conceived of, oversaw and directed the research; analyzed data; obtained research funding; and wrote the manuscript.

Competing interests

G.M.D. and R.M.P. declare competing financial interests and have submitted patents (US patents: 63/223,473 and 63/223,453) for antibody targeting of MCT11 expressing T_{ex} cells that are entitled to a share in net income generated from licensing of these patent rights for commercial development. G.M.D. consults for and/or is on the scientific advisory board of BlueSphere Bio, Century Therapeutics, Nanna Therapeutics, Novasenta, Pieris Pharmaceuticals and Western Oncolytics/Kalivir and has grants from bluebird bio, Novasenta, Pfizer, Pieris Pharmaceuticals, TCR2 and Western Oncolytics/Kalivir. G.M.D. owns stock in Novasenta, BlueSphere Bio and RemplirBio. The other authors declare no competing interests.

Additional information

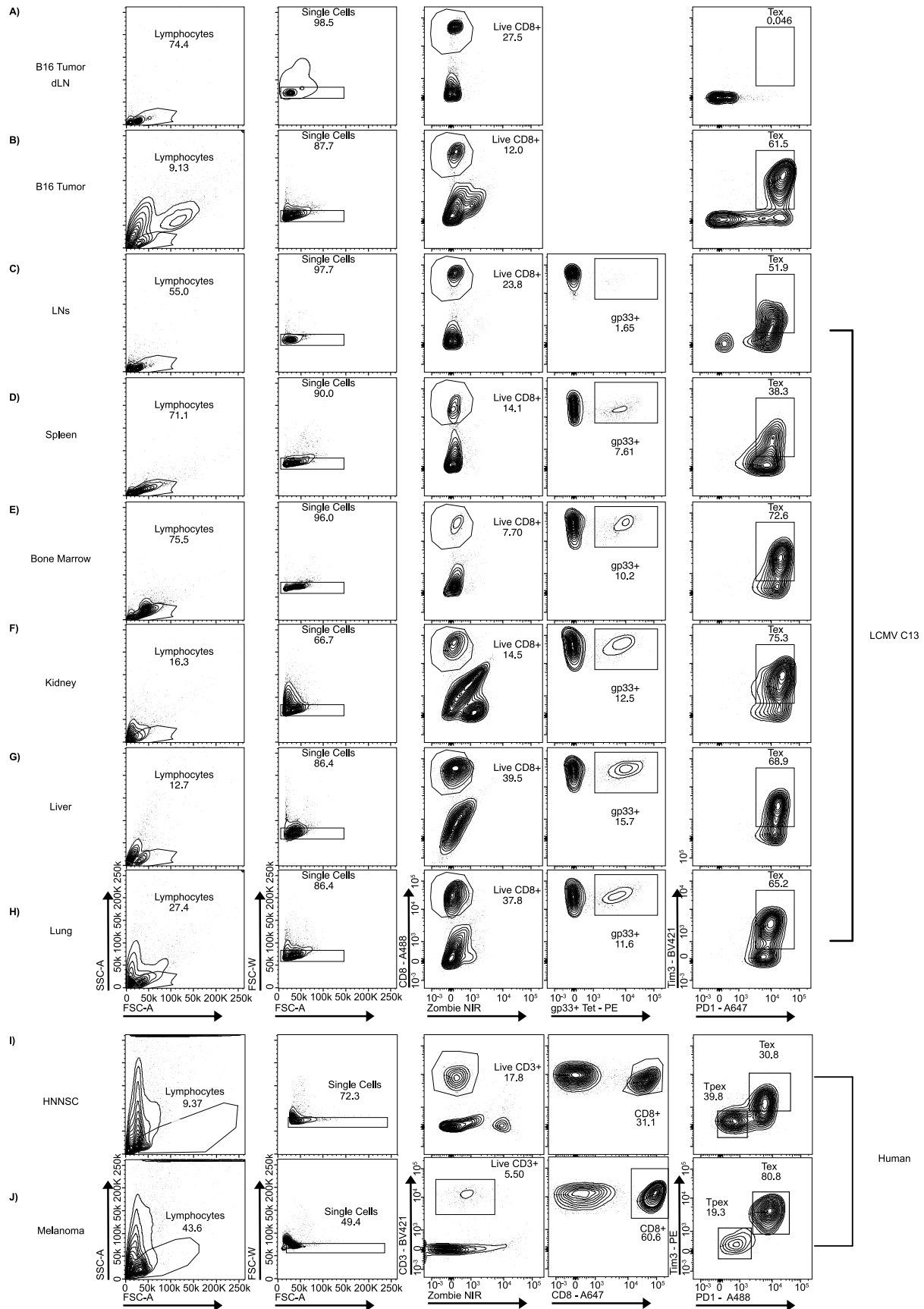
Extended data is available for this paper at <https://doi.org/10.1038/s41590-024-01999-3>.

Supplementary information The online version contains supplementary material available at <https://doi.org/10.1038/s41590-024-01999-3>.

Correspondence and requests for materials should be addressed to Greg M. Delgoffe.

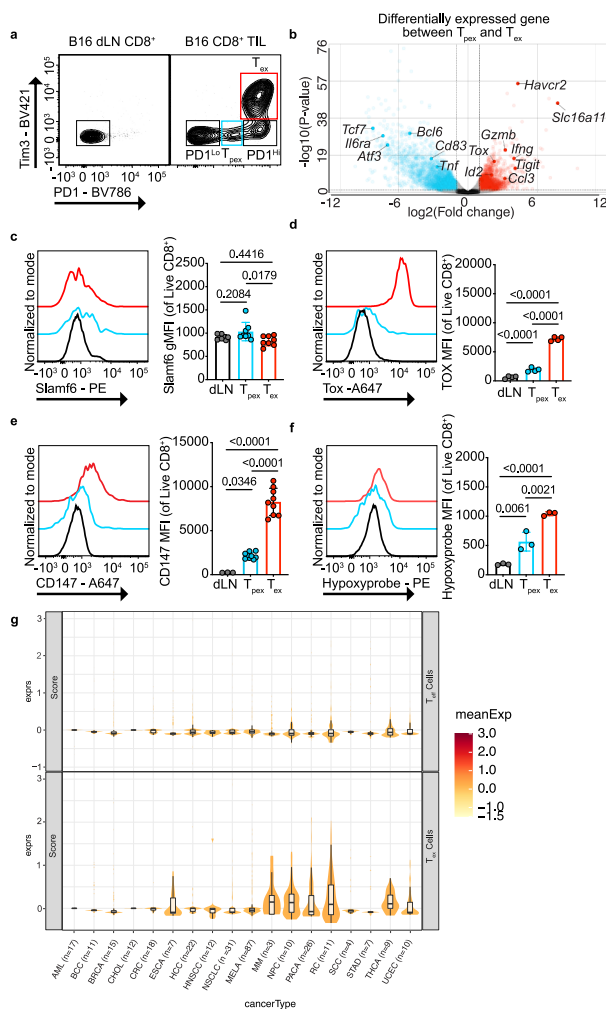
Peer review information *Nature Immunology* thanks Ping-Chih Ho and the other, anonymous, reviewer(s) for their contribution to the peer review of this work. Primary Handling Editor: Nick Bernard, in collaboration with the *Nature Immunology* team.

Reprints and permissions information is available at www.nature.com/reprints.



Extended Data Fig. 1 | Gating strategy in mouse model and human samples. Gating strategy from total sample to live CD8⁺PD1⁺Tim3⁺ T cells from **a)** dLN and **b)** B16 tumors. Gating strategy from total sample to live CD8⁺gp33tet⁺PD1⁺Tim3⁺

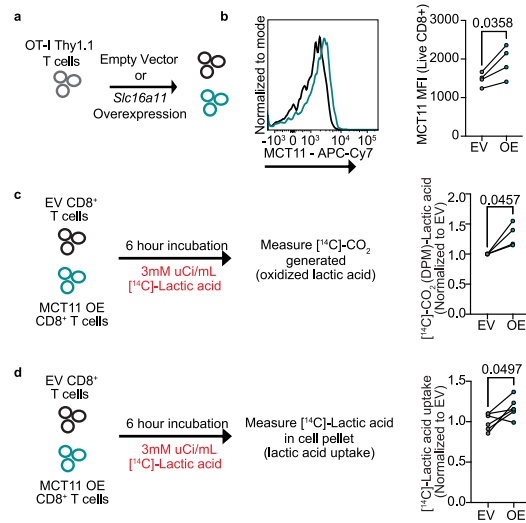
T cells from murine LCMV C13 infected **c)** LNs, **d)** spleen, **e)** bone marrow, **f)** kidney, **g)** liver and **h)** lung. Gating strategy from total sample to live CD8⁺ T cells in **i)** human HNSC and **j)** melanoma.



Extended Data Fig. 2 | Terminally exhausted T cells differentially express solute carriers.

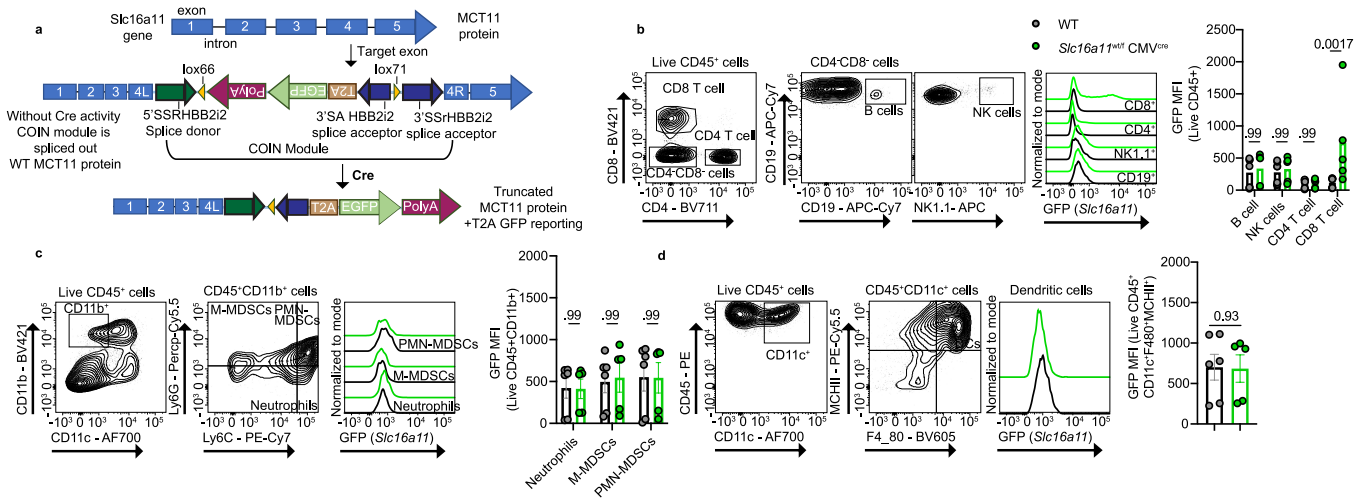
a) Representative flow cytometry plot of PD1 and Tim3 expression on CD8⁺ T cells in day 14 B16 tumors and dLNs. **b**) Volcano plot of differentially expressed genes in progenitor vs terminally exhausted T cells. **c**) Representative histogram and quantification of Slamf6 expression in B16 dLN CD8⁺ T cells, and B16 tumor infiltrating T_{pe} and T_{ex} (n = 8 for all groups). **d**) Representative histogram and quantification of Tox expression in B16 dLN CD8⁺ T cells (n = 4), and B16 tumor infiltrating T_{pe} (n = 4) and T_{ex} cells (n = 4).

e) Representative histogram and quantification of CD147 expression in dLN CD8⁺ (n = 3), and B16 tumor infiltrating T_{pe} (n = 9) and T_{ex} cells (n = 9). **f**) Representative histogram and quantification of hypoxyprobe staining in B16 dLN CD8⁺ T cells (n = 3), and B16 tumor infiltrating T_{pe} (n = 3) and T_{ex} cells (n = 3). **g**) Expression of *SLC16A11* from single cell analysis in human effector and T_{ex} cells in various human tumors. Data represent one (**d,f**) or two (**c,e**) independent experiments. Error bars indicate +/- standard error of mean (SEM). Statistical analysis performed by one way analysis of variance (ANOVA) with Tukey's multiple comparisons test (**c-f**).



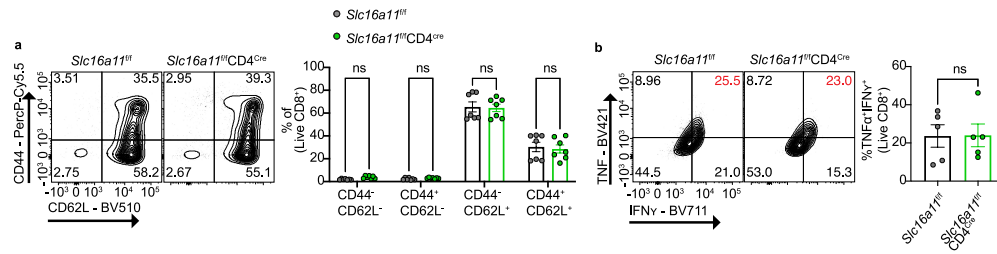
Extended Data Fig. 3 | MCT11 overexpression increases lactic acid metabolism in CD8⁺ T cells. **a**) OT-I T cells were retrovirally transduced with an MCT11 overexpression vector. **b**) Representative histogram and quantification of MCT11 expression in OT-I T cells transduced with EV control plasmid (n = 4) or an MCT11 overexpression plasmid (n = 4). **c**) Experimental outline and quantification of

[¹⁴C]-Lactic acid oxidation experiment in EV (n = 4) or MCT11 OE T cells (n = 4). **d**) Experimental outline and quantification of [¹⁴C]-Lactic acid uptake experiment in EV (n = 6) or MCT11 OE T cells (n = 6). Data represent four independent experiments. Error bars indicate \pm SEM. Statistical analysis performed by paired two-tailed Student's T tests (**b-d**).



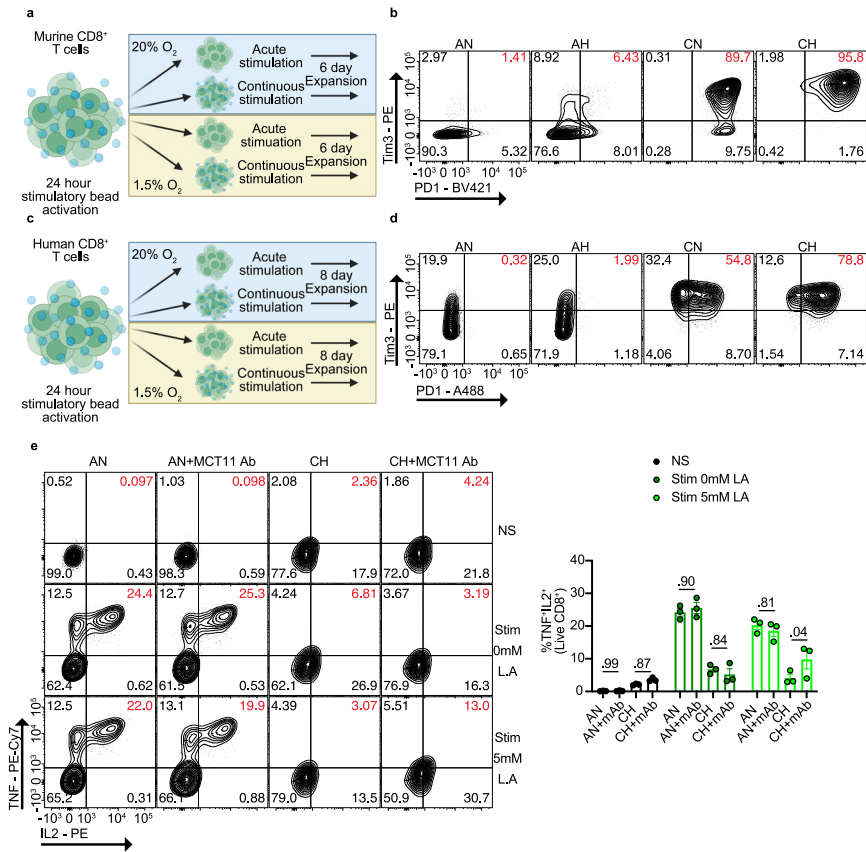
Extended Data Fig. 4 | MCT11 expression is confined to exhausted T cells among tumor infiltrating immune populations. a Cartoon of *Slc16a11* exons in WT and *Slc16a11*^{wt/f} mice where Cre expression leads to the transcription of a truncated MCT11 protein with simultaneous GFP expression. **b** Representative flow cytometry plot, histogram and quantification of MCT11 (via GFP reporter expression) in CD8, CD4, NK and B cells infiltrating B16 tumors on WT (n = 6) and *Slc16a11*^{wt/f}CMV^{cre} (n = 5) mice. **c** Representative flow cytometry plot, histogram

and quantification of MCT11 (via GFP reporter expression) in B16 infiltrating monocytes on WT (n = 6) and *Slc16a11*^{wt/f}CMV^{cre} (n = 5) mice. **d** Representative flow cytometry plot, histogram and quantification of MCT11 (via GFP reporter expression) in B16 infiltrating dendritic cells on WT (n = 6) and *Slc16a11*^{wt/f}CMV^{cre} (n = 5) mice. Data represent two independent experiments. Error bars indicate \pm SEM. Statistical analysis performed by two-way ANOVA with Sidak's multiple comparisons test (**b-c**) or by unpaired two-tailed Student's T tests (**d**).



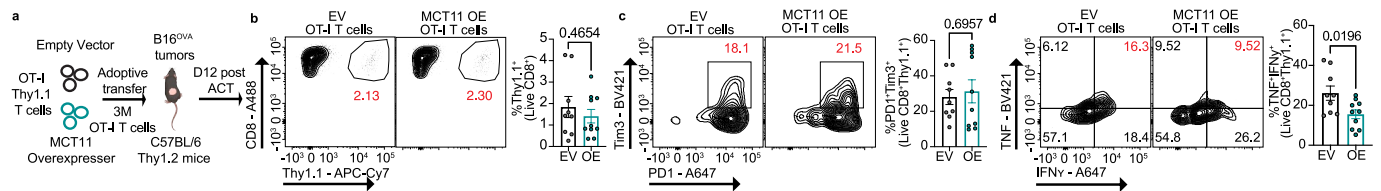
Extended Data Fig. 5 | CD8⁺ T cells from *Slc16a1^{fl/fl}CD4^{Cre}* mice have no developmental or functional differences until they become exhausted. **a) Representative flow cytometry plot and quantification of CD44 and CD62L populations in CD8⁺ T cells isolated from LNs of 10-week-old *Slc16a1^{fl/fl}* (n = 7) and *Slc16a1^{fl/fl}CD4^{Cre}* mice (n = 7) **b**) Representative cytogram and quantification of**

TNF and IFN γ populations in CD8⁺ T cells isolated from LNs of *Slc16a1^{fl/fl}CD4^{Cre}* (n = 5) mice and littermate controls (n = 5). Data represent two independent experiments. Error bars indicate \pm SEM. Statistical analysis performed by two-way ANOVA with Sidak's multiple comparisons (**a**) or by unpaired two-tailed Student's T tests (**b**).



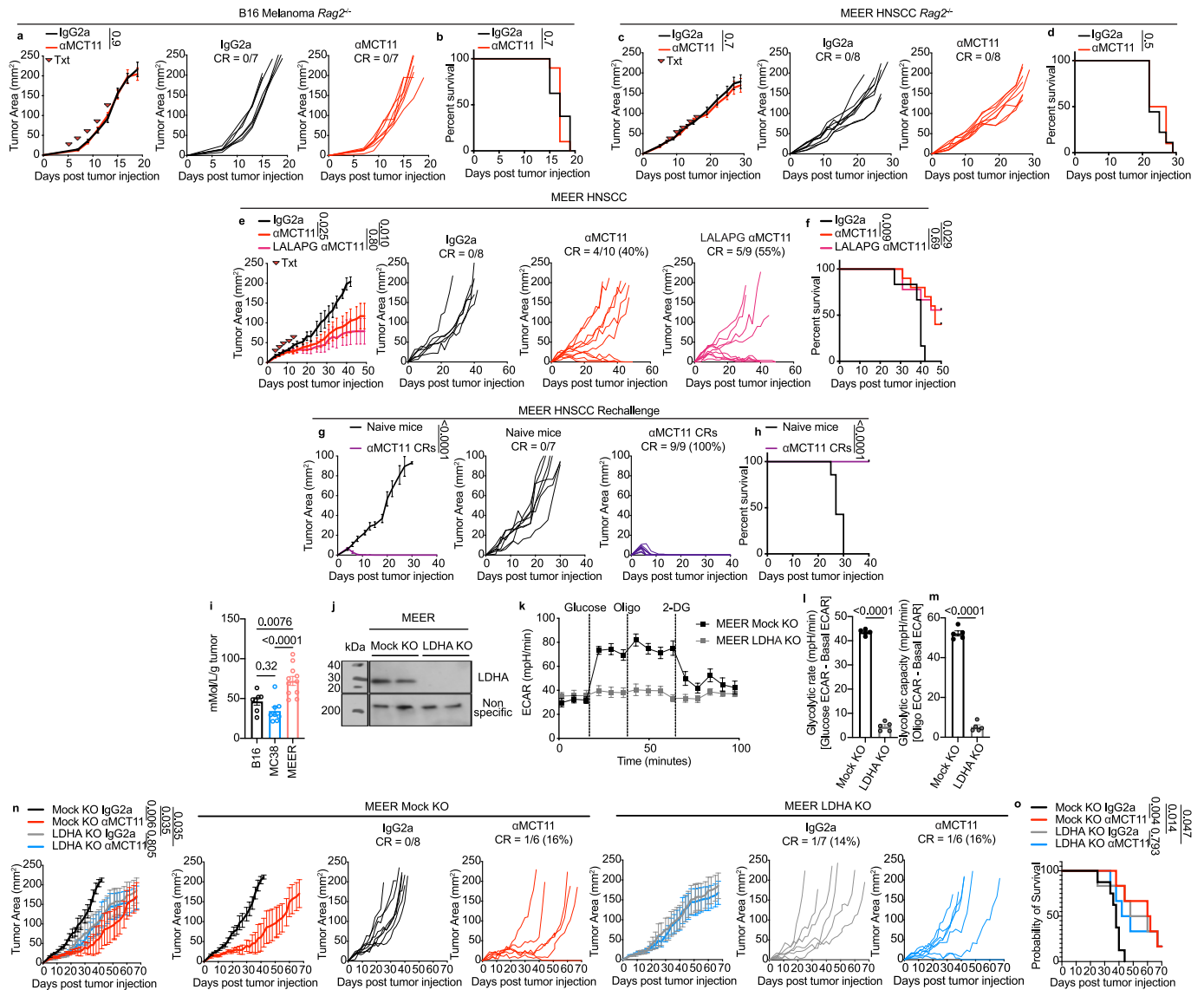
Extended Data Fig. 6 | Continuous stimulation under hypoxia drives an exhaustion-like state. a) Murine CD8⁺ T cells were activated with CD3/CD28 stimulatory beads at a 1:1 ratio for 24 hours, and then expanded for 6 days w/out beads or at a 10:1 (B:T) ratio in 20% O₂ or %1.5 O₂. **b)** Flow cytometry plot of PD1 and Tim3 expression in murine CD8⁺ T cells after 6 days in culture under acute stimulation (A) and normoxia (N), A and hypoxia (H), continuous stimulation (C) and N, or C and H. **c)** Human CD8⁺ T cells were activated with CD3/CD28 stimulatory beads at a 1:1 ratio for 24 hours, and then expanded for 8 days without beads or at a 10:1 (B:T) ratio in 20% O₂ or %1.5 O₂. **d)** Flow cytometry plots of PD1

and Tim3 expression in human CD8⁺ T cells after 8 days in culture in the described conditions. **e)** Representative flow cytometry plot and tabulation of the percent of cells producing TNF and IL2, when stimulated for 5 hours with αCD3 (3 μg/mL) and αCD28 (2 μg/mL) in the presence of 5 mM lactic acid +/- MCT11 antibody (40 μg/mL) (n = 3 for all samples). Data represent one experiment. Error bars indicate +/- SEM. Statistical analysis performed by two-way ANOVA with Tukey's multiple comparison **(e)**. **(a)** Created in BioRender. Peralta, R. (2023) [BioRender.com/r15f775](https://www.biorender.com/r15f775).



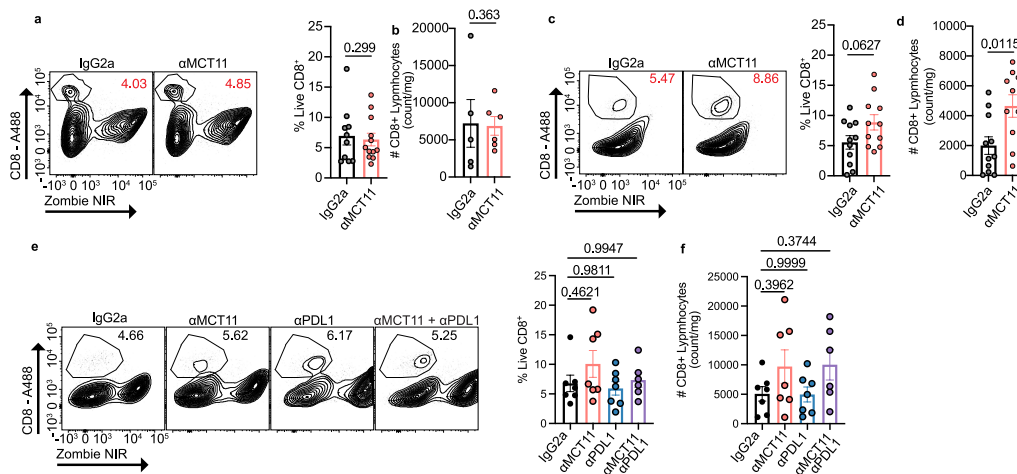
Extended Data Fig. 7 | MCT11 overexpression accelerates T cell dysfunction in the TME. a OT-I Thy1.1 T cells were retrovirally transduced with an MCT11 overexpression vector (OE) or control empty vector (EV), and 3 million T cells were adoptively transferred into day 7 B16^{OVA} bearing C57BL/6 Thy1.2 mice. **b** Representative flow plot and quantification of percentage of CD8⁺Thy1.1⁺ transduced with EV (n = 9) or OE (n = 10) (transferred OT-I)s infiltrating B16^{OVA} tumors. **c** Representative flow plot and quantification of PD1⁺Tim3⁺ population

in adoptively transferred EV (n = 9) or OE (n = 10) OT-I T cells. **d** Representative flow plot and quantification of TNF⁺IFNγ⁺ population in adoptively transferred EV (n = 9) or OE (n = 10) T cells. Data represent three independent experiments. Error bars indicate +/- SEM. Statistical analysis performed by unpaired two-tailed Student's T tests (**b-d**). (a) Created in BioRender. Peralta, R. (2024) [BioRender.com/k52v484](https://www.biorender.com/k52v484).



Extended Data Fig. 8 | α MCT11 therapy requires T cells and is driven by lactate metabolism in cancer. Tumor growth curve and **b**) survival curve of B16 bearing *Rag2*^{-/-} mice treated with isotype control (n = 7) or α MCT11 (n = 7). **c**) Tumor growth curve and **d**) survival curve of MEER bearing *Rag2*^{-/-} mice treated with isotype control (n = 8) or α MCT11 (n = 8). **e**) Tumor growth and **f**) survival curve of MEER bearing mice treated with isotype control (n = 8), α MCT11 (n = 10) or LALAPG α MCT11 (n = 9). **g**) MEER tumor growth and **h**) survival curve of naïve mice (n = 7) and mice rechallenged 1 month after complete responses to MCT11 therapy (n = 9). **i**) Lactate concentrations in TIF of B16 (n = 7), MC38 (n = 8) and MEER (n = 11) tumors. **j**) Immunoblot of LDHA in mock KO and LDHA KO MEER

tumor cells (one experiment). **k**) Extracellular acidification rate plot, **l**) glycolytic rate and **m**) glycolytic capacity in mock KO (n = 5) and LDHA KO MEER (n = 5) tumor cells. **n**) Tumor growth and **o**) survival curves of mice injected I.D. with 250 K mock KO or LDHA KO MEER cells and treated with isotype control or α MCT11 (200 μ g/dose; 5 doses total). Data represent one (**g-h,j**), two (**a-f,k-o**) or three (**i**) independent experiments. Error bars indicate \pm SEM. Statistical analysis performed by paired two-tailed Student's T tests (**l-m**), one way ANOVA with Tukey's multiple comparisons (**i**), Two-way ANOVA with Tukey's multiple comparisons (**a,c,e,g,n**), or by Log Rank Mendel Cox Test (**b,d,f,h,o**).



Extended Data Fig. 9 | Effects of MCT11 therapy on total CD8⁺ T cells in tumors. **a** Representative flow cytometry plot and quantification of percentage of live CD8⁺ T cells infiltrating B16 when treated with isotype (n = 11) or αMCT11 (n = 12). **b** Total counts of CD8⁺ T cells infiltrating B16 when treated with isotype (n = 5) or αMCT11 (n = 6). **c** Representative flow cytometry plot and quantification of percentage and **d** total counts of live CD8⁺ T cells infiltrating MEER when treated with isotype control (n = 11) or αMCT11 (n = 11).

e Representative flow cytometry plot and quantification of percentage and **f** total counts of live CD8⁺ T cells infiltrating MC38 when treated with isotype control (n = 7), αMCT11 (n = 7), αPDL1 (n = 7) or αMCT11 + αPDL1 (n = 6). Data represent two (**a–b**), or three (**c–f**) independent experiments. Error bars indicate \pm SEM. Statistical analysis performed by unpaired two-tailed Student's T tests (**a–b**) or by one-way ANOVA with Tukey's multiple comparison (**c–f**).

Reporting Summary

Nature Portfolio wishes to improve the reproducibility of the work that we publish. This form provides structure for consistency and transparency in reporting. For further information on Nature Portfolio policies, see our [Editorial Policies](#) and the [Editorial Policy Checklist](#).

Statistics

For all statistical analyses, confirm that the following items are present in the figure legend, table legend, main text, or Methods section.

n/a Confirmed

- The exact sample size (n) for each experimental group/condition, given as a discrete number and unit of measurement
- A statement on whether measurements were taken from distinct samples or whether the same sample was measured repeatedly
- The statistical test(s) used AND whether they are one- or two-sided
Only common tests should be described solely by name; describe more complex techniques in the Methods section.
- A description of all covariates tested
- A description of any assumptions or corrections, such as tests of normality and adjustment for multiple comparisons
- A full description of the statistical parameters including central tendency (e.g. means) or other basic estimates (e.g. regression coefficient) AND variation (e.g. standard deviation) or associated estimates of uncertainty (e.g. confidence intervals)
- For null hypothesis testing, the test statistic (e.g. F , t , r) with confidence intervals, effect sizes, degrees of freedom and P value noted
Give P values as exact values whenever suitable.
- For Bayesian analysis, information on the choice of priors and Markov chain Monte Carlo settings
- For hierarchical and complex designs, identification of the appropriate level for tests and full reporting of outcomes
- Estimates of effect sizes (e.g. Cohen's d , Pearson's r), indicating how they were calculated

Our web collection on [statistics for biologists](#) contains articles on many of the points above.

Software and code

Policy information about [availability of computer code](#)

Data collection Data collection utilized BD FACSDiva v9.0 for flow cytometry, Seahorse Wave Controller Software V2.6.3.8 for extracellular flux assays.

Data analysis Data was analyzed with FlowJo V10 and Prism10. Bulk RNA-seq analysis was performed on PartekFlow. Paired end reads were concatenated into a single fastq file. Reads were trimmed for adapters using CutadaptV1.12 before being aligned to Mus musculus reference genome (mm38) using the RNA-seq aligner STAR2.7. Using the raw counts, differential genes were found by DESeq2. Gene set enrichment analyses of selected immunologic signature and hallmark gene sets was performed with clusterProfiler (REF <https://doi.org/10.1016/j.xinn.2021.100141>). Single-cell RNAseq data from blood and tumor infiltrating immune populations from a cohort of head and neck cancer patients was utilized to evaluate the expression of MCT11 across subsets of CDS+ T cells. Feature/barcode expression matrices were downloaded from the Gene Expression Omnibus and cell type annotations were inferred as previously described. CDS+ T cells were then bioinformatically isolated from other immune populations, and the top 2000 highly variable genes were used as input for dimensionality reduction with principal component analysis. The top principal components were identified heuristically by identifying the inflection point on an elbow plot and were subsequently used for generating uniform manifold approximation and projection (UMAP) embeddings and Louvian-based clustering. Co-expression of PDCD1, HAVCR2 and SLC16A 11 was then evaluated across clusters in PBMC and TIL and was visualized with a heatmap.

For manuscripts utilizing custom algorithms or software that are central to the research but not yet described in published literature, software must be made available to editors and reviewers. We strongly encourage code deposition in a community repository (e.g. GitHub). See the Nature Portfolio [guidelines for submitting code & software](#) for further information.

Data

Policy information about [availability of data](#)

All manuscripts must include a [data availability statement](#). This statement should provide the following information, where applicable:

- Accession codes, unique identifiers, or web links for publicly available datasets
- A description of any restrictions on data availability
- For clinical datasets or third party data, please ensure that the statement adheres to our [policy](#)

RNA-seq data have been deposited to the Gene Expression Omnibus (GEO) with accession no. GSE249944. Source data for single cell RNA sequencing are available in the GEO repository, accession no. GSE139324. Source data for Figure 1a-b and Extended Figure 2b, as well as WT control for Figure 3g-h, are available in the GEO repository, accession no. GSE175408.

Research involving human participants, their data, or biological material

Policy information about studies with [human participants or human data](#). See also policy information about [sex, gender \(identity/presentation\), and sexual orientation](#) and [race, ethnicity and racism](#).

| | |
|--|-----|
| Reporting on sex and gender | N/A |
| Reporting on race, ethnicity, or other socially relevant groupings | N/A |
| Population characteristics | N/A |
| Recruitment | N/A |
| Ethics oversight | N/A |

Note that full information on the approval of the study protocol must also be provided in the manuscript.

Field-specific reporting

Please select the one below that is the best fit for your research. If you are not sure, read the appropriate sections before making your selection.

- Life sciences Behavioural & social sciences Ecological, evolutionary & environmental sciences

For a reference copy of the document with all sections, see [nature.com/documents/nr-reporting-summary-flat.pdf](https://www.nature.com/documents/nr-reporting-summary-flat.pdf)

Life sciences study design

All studies must disclose on these points even when the disclosure is negative.

| | |
|-----------------|--|
| Sample size | Sample sizes were not statistically predetermined but were chosen based on previous work in exhausted T cell and tumor immunology (Scharping et al 2016 Immunity, Menk et al 2018 J Exp Med, Scharping et al 2017 Cancer Immunol Res., Najjar et al 2019 Cancer Immunol Res.). These sample sizes are sufficient to allow for the determination of statistical significance between groups and minimized the number of animals or replicates needed for each experiment. |
| Data exclusions | For tumor implantation studies in mice, we excluded data if tumors ruptured and ulcerated prior to the completion of the experiment as this dramatically alters the tumor microenvironment and longitudinal growth. Statistical outliers were determined based on Grubb's outlier test. |
| Replication | Experiments were conducted at least two independent times (and in most cases, at least three independent times) with all attempts of replication being successful. |
| Randomization | Mice were placed into experimental groups and were randomized into treatment types. For experiments with mouse-derived cells, cells were split and each given the same treatment to generate paired data. |
| Blinding | All tumor growth curves were conducted in a blinded manner—one author administered treatments while another independently measured tumor size. For all other experiments, data collection and analysis were not performed blind to the conditions of the experiments. |

Reporting for specific materials, systems and methods

We require information from authors about some types of materials, experimental systems and methods used in many studies. Here, indicate whether each material, system or method listed is relevant to your study. If you are not sure if a list item applies to your research, read the appropriate section before selecting a response.

Materials & experimental systems

| n/a | Involved in the study |
|-------------------------------------|---|
| <input type="checkbox"/> | <input checked="" type="checkbox"/> Antibodies |
| <input type="checkbox"/> | <input checked="" type="checkbox"/> Eukaryotic cell lines |
| <input checked="" type="checkbox"/> | <input type="checkbox"/> Palaeontology and archaeology |
| <input type="checkbox"/> | <input checked="" type="checkbox"/> Animals and other organisms |
| <input type="checkbox"/> | <input checked="" type="checkbox"/> Clinical data |
| <input checked="" type="checkbox"/> | <input type="checkbox"/> Dual use research of concern |
| <input checked="" type="checkbox"/> | <input type="checkbox"/> Plants |

Methods

| n/a | Involved in the study |
|-------------------------------------|--|
| <input checked="" type="checkbox"/> | <input type="checkbox"/> ChIP-seq |
| <input type="checkbox"/> | <input checked="" type="checkbox"/> Flow cytometry |
| <input checked="" type="checkbox"/> | <input type="checkbox"/> MRI-based neuroimaging |

Antibodies

Antibodies used

BioLegend: anti-CD4 (GK1 .5, catalogue number 100412, lot number B184560, dilution 1 :1,000), anti-CDS (53-6.7, catalogue number 100707, lot number B171971, dilution 1 :1,000), anti-CD44 (IM7, catalogue number 103032, lot number B267976, dilution 1 :500), CD45 (13/2.3, catalogue number 147711, lot number B254856, dilution 1:1000) anti-CD147 (OX-114, catalogue number 123716, lot number B262975, dilution 1 :500), anti-CD19 (6D5, catalogue number 115530, lot number B276004, dilution 1:1000), anti-Ly6G (1 AB, catalogue number 127616, lot number B248844, dilution 1 :500), anti-Ly6C (HK1 .4, Catalogue number 128017, lot number B213757, dilution 1 :500), anti-MHCII (M5/114.15.2, catalogue number 107612, lot number B251993, dilution 1 :500), anti-F4 80 (8MB, catalogue number 123149, lot number B326894, dilution 1 :250), anti-CD279 (PD1, 29F.1A12, catalogue number 135221, lot number B194160, dilution 1 :250), anti-Tim3 (RMT3-23, catalogue number 119705, lot number B224472, dilution 1 :250), anti-IFN γ (XMG1 .2, catalogue number 505842, lot number B270630, dilution 1 :250), anti-TNF α (MP6-XT22, catalogue number 506322, lot number B218553, dilution 1 :500), anti-CD11 b (M1/70, catalogue number 101204, lot number B307868, dilution 1 :250), and anti-CD11c (N418, catalogue number 117320, lot number B286499, dilution 1 :250).

Human samples were stained with the following antibodies (BioLegend): anti-PD1 (EH12.2Z7, catalogue number 329904, dilution 1 :200), anti-TIM3 (F382E2, catalogue number 345006, dilution 1 :200), anti-CDS (HIT8a, catalogue number 300918, dilution 1 :200), and anti-CD3 (SK7, catalogue number 344834, dilution 1 :200).

Invitrogen: anti-CD62L (MEL-14, catalogue number 564109, lot number 7341887, dilution 1 :500), and anti-TOX (TXRX10, catalogue number 80-6502-82, lot number 2246902, dilution 1 :250).

Cell signaling: anti-LDHA (catalogue number 2012s, dilution 1:1000)

anti- PD1 (Bio X Cell; Clone RMP1-14; Catalogue:BE0146) &(Bio X Cell; Clone J43; Catalogue:BE0033-2)

MCT11 antibody

Validation

All antibodies and stains are commercially available and were validated by the manufacturer. MCT11 antibody was validated by staining MCT11 overexpressing cells.

Eukaryotic cell lines

Policy information about [cell lines and Sex and Gender in Research](#)

Cell line source(s)

We obtained B16-F10 (CRL-6475) and A549 (CCL-185) cells were obtained from the American Type Culture Collection (ATCC). MC38 cells were obtained from Dario Vignali (commercially available from Kerablast). MEER cells were obtained from Robert Ferris (originally from Jung, Y.-S. et al. CD200: association with cancer stem cell features and response to chemoradiation in head and neck squamous cell carcinoma. Head Neck 37, 327-335 (2015).)

Authentication

The B16, A549 cell line were authenticated in 2018 through independent sequencing by the supplier. The MC38 cell lines was authenticated in 2016 via sequencing by their supplier. MEER cells were generated by overexpressing E6/E7 and Ras in primary mouse tonsil epithelial cells (MTECs), and1 and were authenticated by the supplier in 2013 via western blot to confirm E6/E7 and Ras overexpression.

Mycoplasma contamination

MC38 and MEER were confirmed mycoplasma free in 2016, and A549 and B16 in 2018.

Commonly misidentified lines
(See [ICLAC](#) register)

No commonly misidentified cell lines were used in this study.

Animals and other research organisms

Policy information about [studies involving animals; ARRIVE guidelines](#) recommended for reporting animal research, and [Sex and Gender in Research](#)

Laboratory animals

C57BL/6, -Rag1 $^{-/-}$, CD4cre, OT-I, NSG and -Thy1 a (Thy1 .1 congenic) were purchased from The Jackson Laboratory. Slc16a11f/f were generated by Sebastien Gingras. All mice were housed in specific pathogen free conditions at an ambient temperature of 20-26 C and humidity of 30-70% with a 12:12 hour light dark cycle prior to use. The maximal tumor size of 15mm in any direction was not

exceeded in any experiment. Both male and female mice were used in these studies. Mice used were between the age of six (6) and ten (10) weeks.

Wild animals

N/A

Reporting on sex

Both male and female mice were used in this study

Field-collected samples

N/A

Ethics oversight

Animal housing and studies were done in accordance with the Institutional Animal Care and Use Committee of the University of Pittsburgh (Protocol #23073380)

Note that full information on the approval of the study protocol must also be provided in the manuscript.

Clinical data

Policy information about [clinical studies](#)

All manuscripts should comply with the ICMJE [guidelines for publication of clinical research](#) and a completed [CONSORT checklist](#) must be included with all submissions.

Clinical trial registration

Provide the trial registration number from ClinicalTrials.gov or an equivalent agency.

Study protocol

Note where the full trial protocol can be accessed OR if not available, explain why.

Data collection

Describe the settings and locales of data collection, noting the time periods of recruitment and data collection.

Outcomes

Describe how you pre-defined primary and secondary outcome measures and how you assessed these measures.

Plants

Seed stocks

N/A

Novel plant genotypes

N/A

Authentication

N/A

Flow Cytometry

Plots

Confirm that:

- The axis labels state the marker and fluorochrome used (e.g. CD4-FITC).
- The axis scales are clearly visible. Include numbers along axes only for bottom left plot of group (a 'group' is an analysis of identical markers).
- All plots are contour plots with outliers or pseudocolor plots.
- A numerical value for number of cells or percentage (with statistics) is provided.

Methodology

Sample preparation

For T cell single cell suspension, lymph nodes and spleens of mice were mechanically disrupted with the back of a syringe plunger and filtered through a 70 micron filter (Fisher Brand). For tumor single cell suspensions, whole tumors were injected with 2mg/mL of collagenase type IV, 2U/mL of dispase and 10U/mL of DNAse I (Sigma) in buffered RPMI, and incubated for 20 minutes at 37 degrees Celsius. Tumors were then mechanically disrupted using the back of a syringe plunger and filtered through a 70 micron filter.

Instrument

BD Fortessa

Software

Flowjo V10

Cell population abundance

N/A

Gating strategy

Lymphocytes were gated using FSC-Area vs. SSC-Area. Doublet exclusion was done through comparison of SSC-Width to SSC-

Gating strategy

Area and FSC-Width to FSC-Area. Viable cells were determined with zombie dye, in which cells negative for zombie stain were viable. See Extended Data Figure 1 for detailed gating strategy.

Tick this box to confirm that a figure exemplifying the gating strategy is provided in the Supplementary Information.